THE DEVELOPMENT OF EXTREMELY HIGH-GRADE IGNIMBRITES: THE EFFECTS OF STRAIN HEATING AND IMPLICATIONS OF ASH AGGLUTINATION

by

SAGE KEMMERLIN

A THESIS

Presented to the Department of Earth Sciences
and the Division of Graduate Studies of the University of Oregon
in partial fulfillment of the requirements
for the degree of
Master of Science

June 2021

THESIS APPROVAL PAGE

Title: The Development of Extremely High-Grade Ignimbrites: The Effects of Strain Heating and Implications of Ash Agglutination

This thesis has been accepted and approved in partial fulfillment of the requirements for the Master of Earth Sciences degree in the Department of Earth Sciences by:

Josef Dufek	Chairperson
Leif Karlstrom	Member
Thomas Giachetti	Member

and

Andrew Karduna	Interim Vice Provost for Graduate Studies

Original approval signatures are on file with the University of Oregon Division of Graduate Studies.

Degree awarded June 2021

THESIS ABSTRACT

Sage Kemmerlin

Master of Science

Department of Earth Sciences

June 2021

Title: The Development of Extremely High-Grade Ignimbrites: The Effects of Strain Heating and Implications of Ash Agglutination

The Miocene Grey's Landing ignimbrite is a large ($\geq$ 23,000 km^3), intensely welded, highly rheomorphic extremely high-grade ignimbrite. The cause of rheomorphism can be attributed to syn-depositional strain heating and post-depositional gravitational flow of the deposit, but the relative contributions of both are not fully constrained. We model the Grey's Landing pyroclastic density current as a dilute current under the assumption that the particles do agglutinate. The model informs a one-dimension thermal diffusion model that allows for progressive aggradation of the pyroclastic density current with strain heating. Three different methods to calculate viscosity in the shear zone were used: two from measurements of the Grey's Landing ignimbrite and inferences of magmatic viscosity, and one from the granular viscosity calculated from the multiphase model. The results from the granular viscosity model were the only physically realistic

results but generated virtually no strain heating, implying that post-depositional flow is primarily responsible for rheomorphism.

CURRICULUM VITAE

NAME OF AUTHOR: Sage Kemmerlin

GRADUATE AND UNDERGRADUATE SCHOOLS ATTENDED:

University of Oregon, Eugene

Georgia Institute of Technology, Atlanta

DEGREES AWARDED:

Master of Earth Sciences, 2021, University of Oregon

Bachelor of Science, Earth and Atmospheric Science, 2017, Georgia Institute of Technology

AREAS OF SPECIAL INTEREST:

Geophysics

Geology

PROFESSIONAL EXPERIENCE:

Graduate Employee, University of Oregon, 2018-2021 Graduate Employee,

Georgia Institute of Technology, 2017-2018

Undergraduate Teaching Assistant, Georgia Institute of Technology, 2016-2017

ACKNOWLEDGMENTS

I would like to thank my advisor, Josef Dufek, for his support throughout the years. I would also like to thank my other committee members, Thomas Giachetti and Leif Karlstrom, for helping mentor me in graduate school. Additionally I would like to acknowledge my research group for their constant support and guidance: Eric Breard, Ryan Cahalan, Gabe Eggers, Amelia Winner, Chris Harper, Paul Regensburger, Allison Kubo, PJ Zrelak, and Annika Dechert.

I want to thank my dear friends and family (Mom, Amma, Aspen, Zach, Trouvé, Bowie, Kathy, Amelia, PJ, Aaron, Brittany, Genesee, Benny) for their ever-persistent support and love. Without you, I would not be here. I love you all immensely and am forever grateful to have you in my life.

I also want to acknowledge that I am an occupier of the traditional homelands and political territories of the Kalapuya People, the First Peoples of the Willamette Valley. Following treaties between 1851 and 1855, Kalapuya People were dispossessed of their homeland by the United States government and forcibly removed to the Coast Reservation in Western Oregon. Descendants of the Kalapuyan tribes are now citizens of the Confederated Tribes of Grand Ronde and the Confederated Tribes of Siletz Indians.

Finally, I acknowledge that my site of study, called Grey's Landing, is located on the traditional homelands of the Shoshone-Bannock Tribes, the Newe (West-

ern Shoshone) whose descendants are members of the Te-Moak Tribe of Western Shoshone Indians, and the Goshute whose descendants are members of the Confederated Tribes of Goshute Reservation.

This thesis is dedicated to Kathy Trafton, my best friend and, as you say, plutonic love of my life. I am forever grateful of you and your friendship.

Kathy, without you I would have never been able shift how I carry the weight of my compounding traumas; never been able to grow despite the weight; never been able to see outside of it to be proud of my growth. Your fierce kindness has shown me how to follow suit and to treat myself with dignity and to demand that others treat me likewise. I had never considered myself anything but a meek person before I met you. Over the course of these past three years, you have inspired me so immensely that I am altered forever. I now have strength and courage I never thought possible before. I now am more outspoken that ever. I am kinder than ever. I am constantly growing because of how much you inspire me and encourage me.

Your friendship has shown me what true, unconditional love is. Our friendship is one that has us constantly bouncing back and forth, encouraging each other to be the best person we can be. It's one where we will go to the mat for each other (and we have so many times).

This thesis is dedicated to you, Kathy. Without you, I don't think I'd have made it through any of this. And I know I wouldn't be the person I am today. I love you so much, my chaotic, passionate, brave, brilliant friend.

TABLE OF CONTENTS

LIST OF FIGURES

LIST OF TABLES

Table Page

CHAPTER I: INTRODUCTION

Extremely high-grade ignimbrites are the enigmatic deposits of a subset of pyroclastic density currents (PDCs), often generated by large explosive eruptions with high temperatures and low water contents (Branney, 2002; Branney et al., 2008), can reach volumes up to hundreds of cubic kilometers. They are commonly thick, extremely-welded, and can display rheomorphic features (e.g. ductile folds, flow banding, elongation lineations, and eutaxitic fabric) caused by rapid ductile deformation in the deposit. A high degree of welding and rheomorphic features are not found in the more common lower-grade ignimbrites (Branney, 2002; Branney and Godchaux, 2004; Robert et al., 2013; Andrews, 2011; Chapin, 1979). Eruptions that produce extremely high-grade rheomorphic ignimbrites have not been witnessed historically (Andrews, 2011).

Rheomorphic ignimbrites occur in a range of diverse settings including intra-continential (e.g.Snake River Plain ignimbrites, Idaho, USA; B and GP (1982)), intra-oceanic (e.g. Mogán and Fataga Formations, Gran Canaria; Schmincke (1974)), rifted continental margin (e.g. Paraná volcanic province, Brazil; Kirstein et al. (2001), and continental arcs (e.g. Bad Step Tuff; Branney and Kokelaar (1992). Rheomorphism is shown by the presence of ductile folds and elongation lineations (Andrews, 2011). The majority of welded ignimbrites are not rheo-

morphic, and many of those that are rheomorphic are only so locally (e.g. Long Top Tuffs; Branney and Kokelaar (1994), Rattlesnake Tuff; Streck and Grunder (1995)). Rheomorphic ignimbrites are particularly abundant in provinces that record the continental rhyolitic volcanism, "Snake River-type" volcanism. This volcanism is characterized by: (1) extensive layers of stratified ash rather than typical Plinian pumice-fall layers; (2) unusually long and large-volume rhyolite lavas rather than typical small rhyolite domes and coulees; (3) ignimbrites that are better sorted and contain less pumice lapilli (or fiamme) than is typical of ignimbrites elsewhere; and (4) ignimbrites that are more intensely rheomorphic and predominantly lava-like than is typical elsewhere (Branney et al., 2008; Andrews, 2011).

For rheomorphism to occur, whether it be during deposition of the pyroclastic density current or in post-depositional remobilization, substantially high temperatures must be reached (900-1000 ^{o}C) or the current must be rapidly deposited (Andrews, 2011; Ekren et al., 1984; Bachmann and Lipman, 2000; Lavallée et al., 2015). Rheomorphism is favored by "soft" pyroclasts of low-viscosity (Andrews, 2011). The mechanisms which lends to the development of extremely high-grade ignimbrites are not fully constrained. The current model is in which progressive aggradation of a pyroclastic density current, syn-depositional shearing in the growing deposit, and gravitational compaction and slumping, lends to the conditions necessary to create widespread rheomorphism (Branney and Kokelaar, 1992;

Branney, 2002; Andrews, 2006, 2011; Robert et al., 2013; Lavallée et al., 2015; Ellis et al., 2015; Knott et al., 2016). Previous studies have aimed to quantify the history and formation of widespread rheomorphism in extremely high-grade ignimbrites, such as the Grey's Landing ignimbrite (Robert et al., 2013; Andrews, 2011; Lavallée et al., 2015; Manley and Andrews, 2004). However, the significance of agglutination of partially molten ash particles on the dynamics of large, hot pyroclastic density currents during both transport and progressive aggradation deposition is relatively little understood.

CHAPTER II: GREY'S LANDING IGNIMBRITE

I want to take this space to acknowledge that the ignimbrite of study, called Grey's Landing, is located on the traditional homelands of the Shoshone-Bannock Tribes, the Newe (Western Shoshone) whose descendants are members of the Te-Moak Tribe of Western Shoshone Indians, and the Goshute whose descendants are members of the Confederated Tribes of Goshute Reservation.

The Miocene Grey's Landing ignimbrite is an intensely welded, extremely high-grade a super-eruption deposit ($\geq 23,000$ km^2) in the central portion of the Snake River Plain in the 15-km-wide Rogerson Graben, Idaho, located in the Yellowstone hot-spot track as shown in Figure 1 (Andrews et al., 2008; Knott et al., 2016, 2020). Knott et al. (2020) estimated eruption volume dense-rock equivalent to be $\geq 2,800$ km^3 with an eruption magnitude of 8.8, making Grey's Landing the largest documented eruption in the Snake River Plain province. There is no evidence of any significant break during the emplacement of the ignimbrite and is inferred to record a single eruption(Andrews, 2011). The deposit, which ranges in thickness from 5 to greater than 100 meters, exhibits rheomorphic and lava-like features (Andrews, 2011; Knott et al., 2020). The ignimbrite rapidly pinches out southwards from the Snake River Plain and west of the Rogerson Graben. Within the graben, which is bound by two normal faults, the Grey's Landing ignimbrite is entirely welded and intensely rheomorphic even as it thins eastward from being $>$ 65 m thick to 4 m thick (Knott et al., 2016; Andrews et al., 2008).

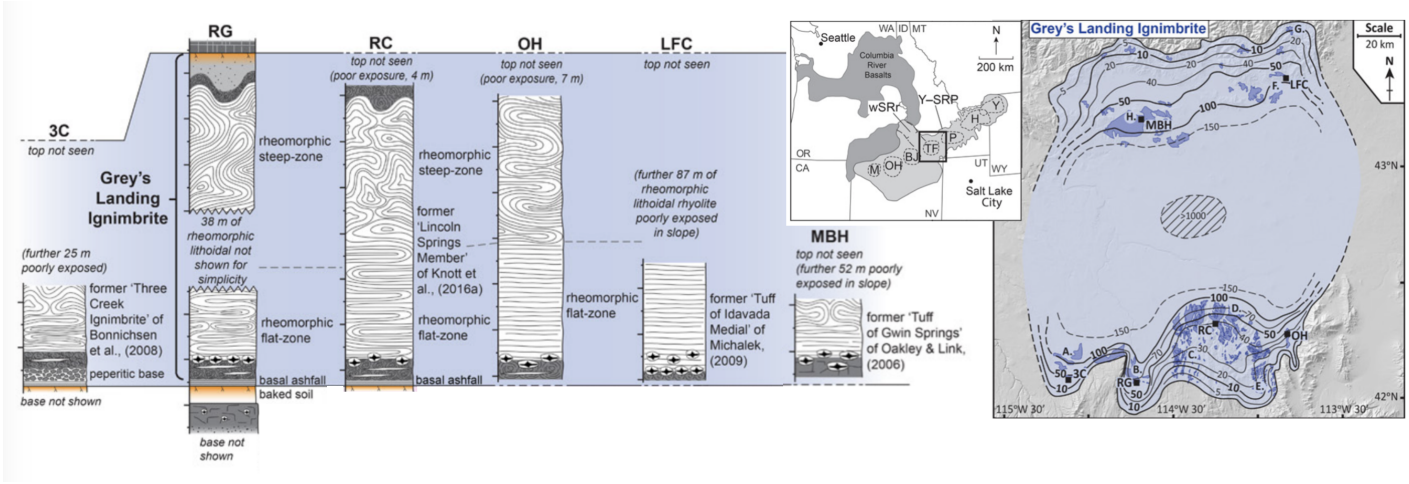

Figure 1: Stratigraphic sections Grey's Landing Ignimbrite and regional map (left) and isopach map (right), modified from Knott et al. (2020), depict the extent of the Grey's Landing ignimbrite. Stratigraphic sections, drawn by Knott et al.(2020) at their field sites (black squares). Site abbreviations: 3C—Three Creek; RG—Rogerson graben; RC—Rock Creek, Cassia Hills; OH—Oakley Hills; LFC—Little Fish Creek, Lake Hills; MBH—Mount Bennett Hills. The regional map (middle insert) illustrates the Yellowstone- Snake River volcanic province (Y-SRP) in the northwesten United States. The image shows rhyolitic eruptive centers: M—McDermitt; OH—Owyhee-Humboldt; BJ—Bruneau-Jarbidge; TF—Twin Falls; P—Picabo; H—Heise; Y—Yellow- stone. Other: wSRr—western Snake River Plain. State abbreviations: WA—Washington; ID—Idaho; MT—Montana; OR—Oregon; CA—California; NV—Nevada; UT—Utah; WY—Wyoming. The black square highlights were Knott et al. (2020) conducted field work. Grey's Landing is located in the Twin Falls (TF) eruptive center. The isopach map shows the thickness distribution of the Grey's Landing ignimbrite in meters.

The paleotopography, on-top of which Grey's Landing was emplaced, is not a uniform, flat surface. The Rogerson Graben, in which much of the ignimbrite sits, developed between 12 and 8 Ma, during which Grey's Landing, and other members of the Rogerson Formation were emplaced (Nash et al., 2006; Bonnichsen et al., 2008). The Rogerson Graben is bound by two formal faults: (1) the 30-km-long Brown's Bench Fault in the west that produced the 400-m-high Brown's Bench escarpment and (2) the smaller Shoshone Hills Fault in the east (Figure 2). These faults were both active at that time. At the time the Grey's Landing ignimbrite was emplaced, the graben floor was west-sloping due to the Brown's Bench Fault (Andrews et al., 2008; Knott et al., 2016). This lead to thickening of the deposit to the west and thinning to the east (Figure 2). Andrews et al (2011) and Knott et al. (2016) argue that the west-sloping graben floor is constistent with W-trending extensional rheomorphic lineations in the Grey's Landing ignimbrite and suggests top-to-the-west downslope rheomorphic shear.

Andrews and Branney (2011) determined four units in the deposit: (1) basal vitrophyre, (2) lithoidal lava-like rhyolite, (3) thin upper vitrophyre, and (4) a sometimes-present non-welded ash top (Figure 1). The ignimbrite is pervasively rheomorphic throughout the entire deposit, including in the lower and upper vitrophyres, with recorded strains of 10-1000 based on estimates from stretched vesicles (Robert et al., 2013; Andrews et al., 2008; Andrews, 2011). The ignimbrite records progressive aggradation of the pyroclastic density current (Branney and Kokelaar,

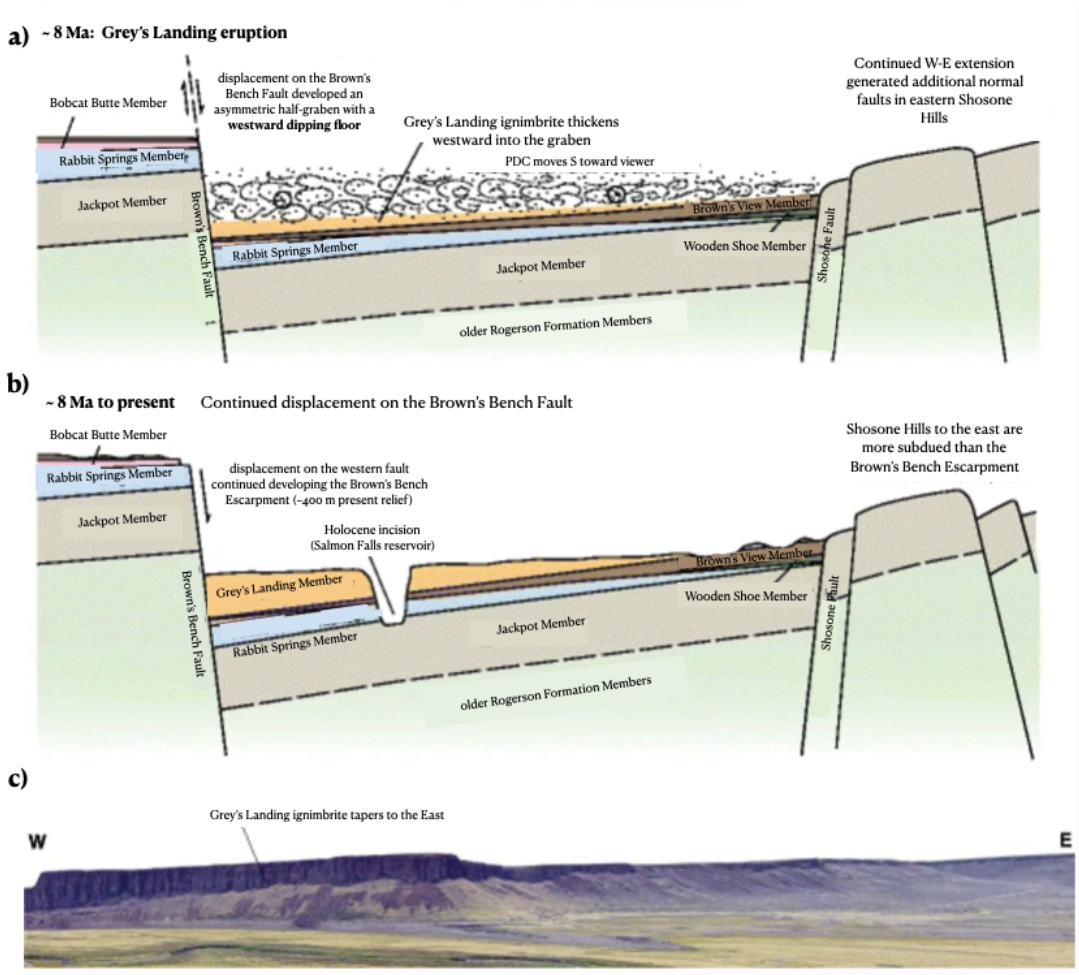

Figure 2: Diagram from Knott et al. (2016). Tectonic evolution of the Rogerson Graben as a series of progressive stages (from 10.59 to 8.0 Ma; (a–b) that account for lateral thickness variations of ignimbrites of the Rogerson Formation. (c) Eastward thinning of the Grey's Landing Member at Backwaters.

1992; Knott et al., 2016; Andrews, 2006, 2011; Robert et al., 2013; Lavallée et al., 2015; Ellis et al., 2015), in which a vertically migrating shear zone produced pervasive extensional lineation, mylonite-like fabrics, folds, and subparallel intrafolial sheath folds (Knott et al., 2016; Andrews, 2011). Gravity-driven deformation, due to maintained hot temperatures (above the glass transition temperature) continued post-deposition, folding the fabric and causing local autobrecciation in the upper vitrophyre which cooled more rapidly (Knott et al., 2016; Andrews, 2011).

Snake River-type ignimbrites (Branney et al., 2008) are inferred to have low magmatic water contents ($<$ 1.5 wt.%) (Almeev et al., 2012). The bulk compositions of the Grey's Landing ignimbrite are rhyolitic, ranging from 73.4 to 75.8 wt. % SiO_2, and are broadly compositionally homogeneous in both the horizontal and vertical directions (Ellis et al., 2013; Bonnichsen et al., 2008; Ellis et al., 2015). The trace elemental composition of the rhyoltic glass in the dense basal and upper vitrophyre are identical, indicating little compositional zonation in the magma prior to eruption (Ellis et al., 2013, 2015). The trace element abundances in the glasses are 45-87 ppm Sr, 1050-1230 ppm Ba, and Li of 21-26 ppm in the basal vitrophyre glass and 17-26 ppm in the upper vitrophyre glass (Ellis et al., 2015). Ellis et al. (2015) also analyzed the plagioclase from the basal and upper vitrophyres and from microcrystalline interior of the ignimbrite. All the trace elements, with the exception of lithium remained consistent throughout the section of deposit. In the plagioclase from the vitrophyres and glassy fallout, Li ranges in

concentrations from 2 to 10 ppm. In the crystallized interior of the ignimbrite, the lithium content reached 68 ppm with an average of 33 ppm. The variation showed no correlation with any other trace element. Ellis et al. (2015) suggest that the variation in Li could be due to diachronous cooling in which the vitrophyres cooled quickly, capturing conditions immediately at emplacement of deposit, before the interior in which Li content may capture a more complicated suite of processes.

The Grey's Landing ignimbrite is one of the most thoroughly studied extremely high-grade ignimbrites. Previous studies have aimed to constrain the duration of post-depositional rheomorphic, lava-like deformation by utilizing one-dimension thermal conduction models. These studies calculated durations of less than 2 years to 16 years (Robert et al., 2013; Andrews, 2011; Manley and Andrews, 2004; Andrews, 2006; Lavallée et al., 2015; Ellis et al., 2015). Variability in the calculated values are due, in part, to the input of different emplacement temperatures as well as due to the incorporation of strain heating. Eruption temperature is the prime control on the emplacement temperature of a deposit (Freundt, 1999). Mineral thermometry suggests magmatic temperatures of $\geq$ 850 °C (Andrews, 2011; Robert et al., 2013; Cathey and Nash, 2004).The high temperatures reached in the ignimbrite have been attributed to either high emplacement and eruption temperatures of approximately 900 to 1,000 °C (Andrews, 2011; Manley and Andrews, 2004) or to lower end member emplacement temperatures of 850 °C where additional heat is generated from shearing in deposit by the overriding pyroclastic

density current (Robert et al., 2013), shown conceptually in Figure 3.

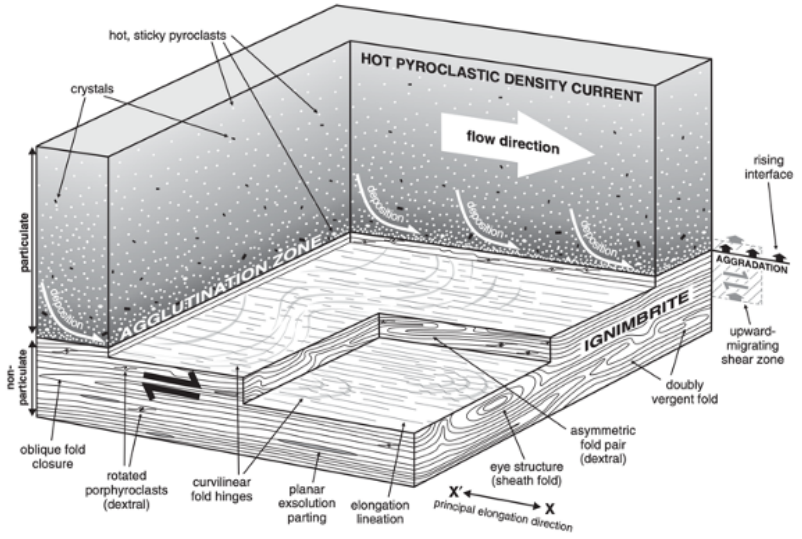

Figure 3: Diagram from Andrews and Branney (2011) depicting the deposition of hot pyroclasts in a pyroclastic density current. Particles deposit, agglutinate, and deform from shearing induced by the overriding current; thus, a vertically migrating shear zone occurs and produces rheomorphic features.

Andrews and Branney (2011) concluded that welding and early deformation in the Grey's Landing ignimbrite occurred rapidly during the deposition of a $\geq$ 1000 °C high-mass-flux PDC. They assume deposition through progressive aggradation of the PDC, creating a $\leq$ 2 m thick vertically-migrating shear zone which produced and deformed the rheomorphic fabric. They argue that deformation continued post-depositionally from viscous spreading and downslope, gravity-induced flow. They argue for cooling of the entire deposit to below the glass transition

temperature (525-750 °C) in much less than two years (Manley and Andrews, 2004; Andrews, 2006), using a one-dimensional conductive cooling model (Manley, 1992). However, Andrews (2006) found the maximum duration of ductile behavior (time above the glass transition temperature) to be 4 years for the ignimbrite at 30 m thickness, and 16 years for the ignimbrite at 60 meters thickness, with ductile behavior in the lower and upper vitrophyres of ≤ 1 year.

Robert et al. (2013) utilized a one-dimensional instantaneous emplacement thermal conduction model to investigate the effects of strain heating on the deposit, while assuming that the deposit in actuality was formed through progressive aggradation. Their viscosity measurements showed a high deposition temperature of > 900 °C or 850 °C if melt contained come dissolved water (0.1 wt. % H_2O). They found possible shear zone residence times of 2-20 hours. They found strain heating of at least a few tens of degrees to be possible and resulted in peak temperatures of 1030-1100 °C.

The Lavallée et al. (2015) study also assumed instantaneous emplacement of Grey's Landing with no deformation during emplacement. They note that these assumptions are simplifications as they believe deposition of pyroclastic density currents results from progressive aggradation and deposits can experience deformation during this process (Branney and Kokelaar, 1992). Their model, a thermal conduction model, assumes an initial homogeneous temperature and porosity, which they allow to evolve over time. Their welding timescale of the

basal vitrophyre agrees with the 12-20 minutes proposed by Robert et al. (2013). They propose that little cooling took place during eruption and transport unless strain heating accommodated for the temperature lost from cooling.

Ellis et al. (2015) utilized a one-dimensional finite difference cooling model with crystal growth to model the thermal evolution of the Grey's Landing ignimbrite. They found a strong contribution of latent heat during the crystallization process, however latent heat only affected profiles where the temperature was maintained long enough for crystals to grow, suggesting a cooling rate between $10^{-2.8}\ Ks^{-1}$ and $10^{-4.5}\ Ks^{-1}$ for the crystalline lithology (Ellis et al., 2015; Lavallée et al., 2015). Their modeling results were in agreement with Lavallée et al. (2015) in that the glassy upper and lower vitrophyres passed below the glass transition temperature and out of the "rheomorphism window" quickly (Figure 4. Their modeling results showed that it is possible that the vitrophyres cooled rapidly but the interior of the ignimbrite remained hot and above the glass transition temperature for far longer (Romine et al., 2012; Ellis et al., 2015). In one calculation they found in slightly less than two years, the vitrophyres cooled to less than 500 °C, while the interior of the deposit remained above 900 °C The suggest, similar to Andrews (2006), that the hot interior of the ignimbrite could flow laterally and could develop rheomorphic folding where the deposit overlaid paleoslopes (Andrews, 2011; Knott et al., 2016).

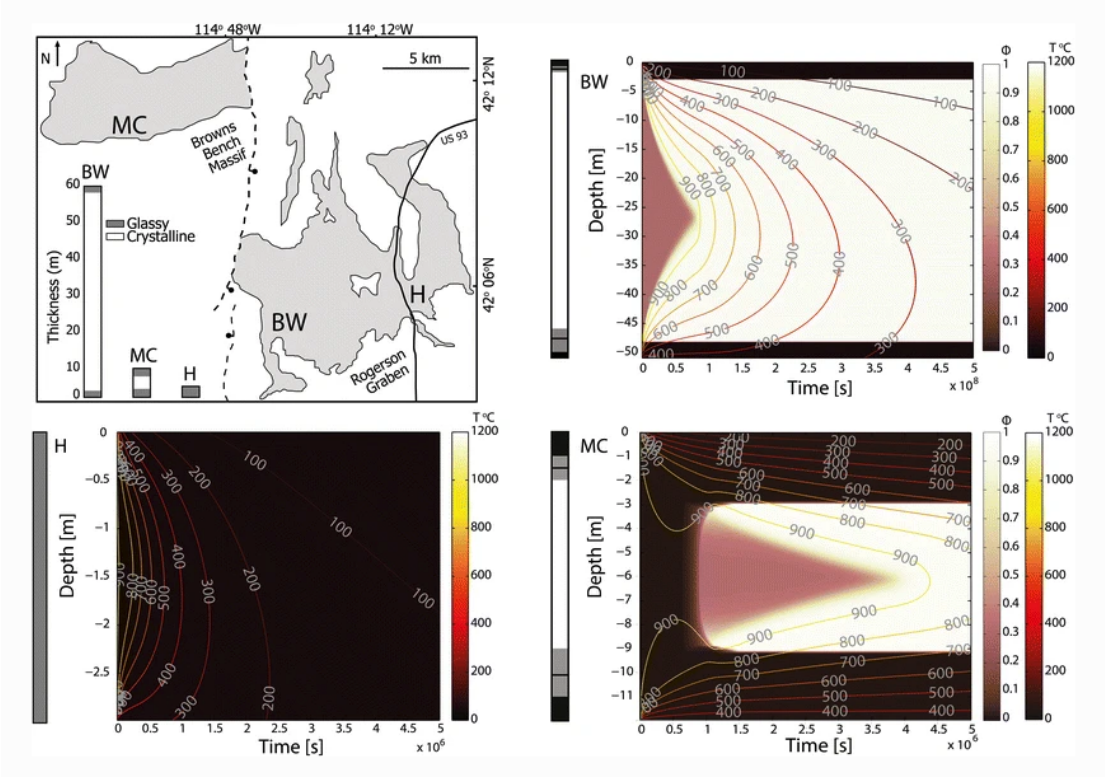

Figure 4: Diagram from Ellis et al. (2015) illustrating the results of their crystal model for three locations with different thicknesses of Grey's Landing. Black indicates amorphous material, and white indicates fully crystalline material while temperature contours illustrate the temperature of the relative positions in the ignimbrite as a function of time.

In regard to the Grey's Landing ignimbrite, a rheomorphic ignimbrite with great areal extent ($\geq$ 23,000 km^2), there is the question of how the pyroclastic density current was able to travel to such extents if the eruption temperature was indeed 900 - 1,000 °C and ash was partially-to-fully molten (Andrews, 2011; Manley and Andrews, 2004; Freundt, 1999). If instead eruption temperatures were lower (850 °C), would strain heating be able to produce high enough temperatures to reach those recorded in the deposit (Robert et al., 2013)? Following gas fluidization experiments using polyethyleneglycole (PEG) powders heated above minimum sintering and melting temperatures, Freundt (1998) concluded that extended particulate transport is only possible if the pyroclastic density current is in a dilute state where aggregation is avoided by a reduced number of particle collisions. However, a dilute and turbulent current would cool rapidly due to entrainment and mixing with cool ambient air (Andrews, 2014; Branney, 2002; Benage et al., 2016). In turn this would reduce the flow's ability to retain high eruption temperatures and reduce the ability to generate rheomorphism without significant heat generated from shear (Freundt, 1998). This study will illuminate the dominant controls on the high temperatures recorded in Grey's Landing and will give insight into the role ash agglutination plays on the development of extremely high-grade ignimbrites.

CHAPTER III: SCALING

We investigate if partially molten ash particles will agglutinate upon deposition by studying the collisional interaction of partially-to-fully molten particles with a flat substrate using scaling relationships. For particle-substrate collisions, where the radius of the substrate (R) can be considered infinite relative to the radius of a particle (R), it scales equivalently to that of two colliding particles each with a radius of $2R$ (Chesters, 1991). In earth science and other fields, such as chemical and process engineering, there are limited studies on the collisions of particles or droplets composed of highly viscous fluids. We therefore utilize two different scaling approaches to determine if results were consistent (Kavehpour, 2015; Freundt, 1998; Janssen, 2011; Telling and Dufek, 2012).

1 Scaling of liquid film-coated particle collisions

We first follow the analysis of the head-on collision of liquid-film-coated particles as laid out in an experimental study of particles impacting a wet surface by Gollwitzer et al. (2012). This approach has previously been applied to water-coated ash to determine a likelihood of aggregation (Telling and Dufek, 2012). The scaling explores the relationship between the wet and dry coefficients of restitutions by characterizing the energy dissipation during an impact. Figure 5 shows the assumed collisional geometries and the potential outcomes of the scaling.

The restitution coefficient can be used to describe if agglutination will occur.

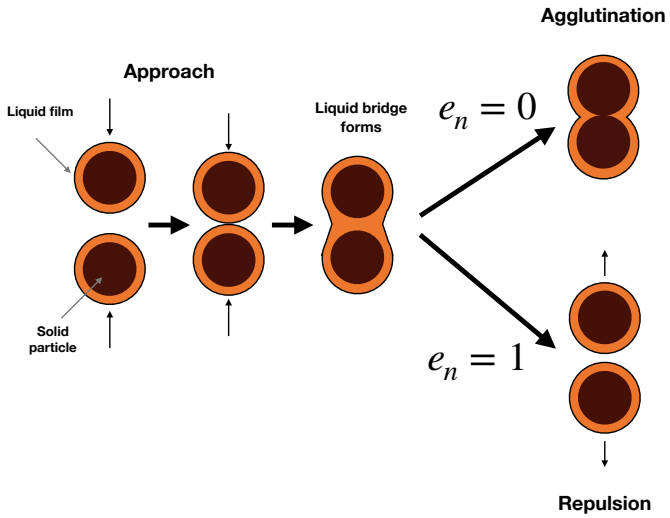

Figure 5: Illustration of the assumed collisional geometry in the Gollwitzer et al. (2012) scaling. Particles are assumed to collide head-on and form a liquid bridge, and then either agglutinate or repel based on the energy of dissipation, the collisional kinetic energy, and the dry restitution coefficient.

At a value of 0 agglutination occurs; whereas at a value of 1, the particles behave perfectly elastically and rebound (Telling and Dufek, 2012; Gollwitzer et al., 2012). The dry 'intrinsic' restitution coefficient (e_o) is determined experimentally by dropping solid particles onto a substrate of the same material. The wet, film-coated, restitution coefficient, relative to the dry restitution coefficient is described by:

$$e_n = \sqrt{e_o^2 - \frac{E_{diss}}{E_i}}, \tag{1}$$

where E_i as the collisional kinetic energy and E_{diss} is the energy of dissipation. The dissipation energy is the sum of 1) the kinetic energy required to move interstitial fluid out of the way of the colliding particle, 2) the viscous dampening experienced by the particle due to the fluid, and 3) the energy required to rupture the capillary fluid bridge during particle rebound (Telling and Dufek, 2012; Gollwitzer et al., 2012).

We apply this scaling to the Grey's Landing ignimbrite-forming pyroclastic density current and additionally use a wide parameter space of differential velocities and liquid film viscosities to compare partially molten ash to a range of collisional interactions. To examine the aggregation potential in the context of viscous and inertial interactions of particles in the flow we use the non-dimensional Stokes and Reynolds number. The particle Stokes number (St_p), the ratio between the inertia of a particle and the viscosity of the liquid, is described by:

$$St_p = \frac{\rho_p d u}{9\mu}, \tag{2}$$

where ρ_p is the density of the solid particle, d is the diameter of the solid particle, u is the differential velocity of the particles, and μ is the viscosity of the liquid film (Gollwitzer et al., 2012). The particle Reynolds number (Re_p), is described by:

$$Re_p = \frac{\rho_l d u}{\mu}, \tag{3}$$

where ρ_l is the density of the liquid film. We utilize a particle diameter of 1 millimeter, a roughness of 1 x $10^{-}8$ m, and a solid ash particle density of 2580 kg/m^3 and molten ash density of 2390 kg/m^3 calculated using the composition of the Grey's Landing ignimbrite in MELTS (Gualda et al., 2012; Ghiorso and Gualda, 2015; Ellis et al., 2013, 2015). We calculate the viscosity, particle Stokes number, particle Reynolds number, associated energies, and restitution coefficient over a range of velocities from 0.01 to 10 m/s. The particle Reynolds number and particle Stokes number for Grey's Landing were on the order of 10^{-6} and 10^{-7}, respectively. The results of the scaling imply that the melt-coated particles will agglutinate with the substrate, as shown below in Figure 6. The value for the wet restitution coefficient for partially molten ash particles is 0.

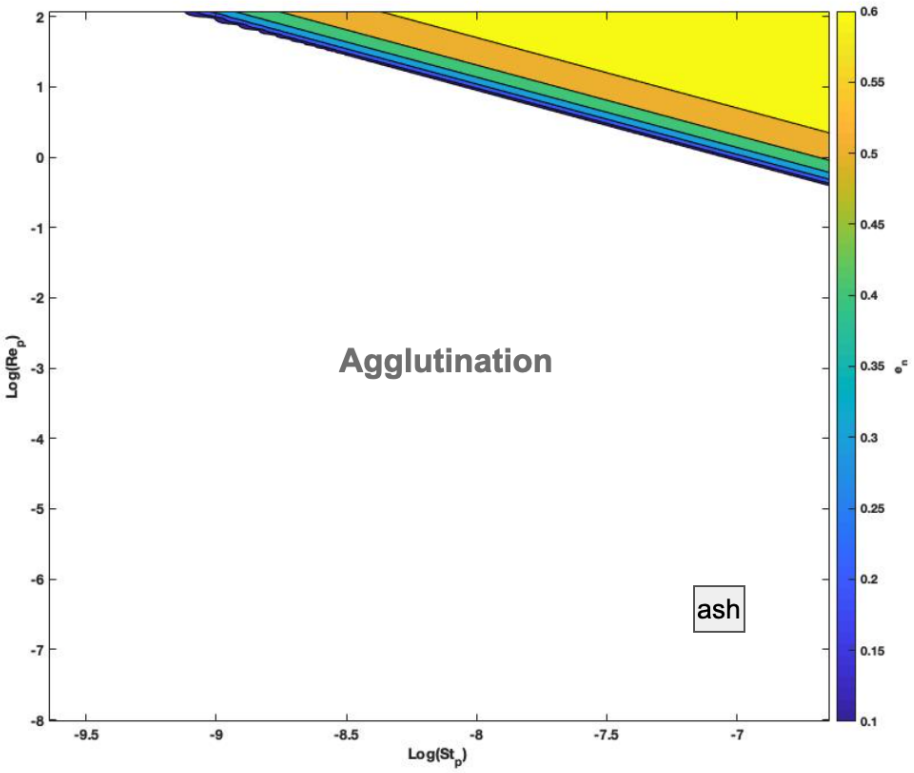

Figure 6: The restitution coefficient plotted as a function of the particle Reynolds and Stokes numbers. Solid, fully molten, and partially-molten ash from Grey's Landing scales in the agglutination space (colored as white here) where the restitution coefficient is 0.

2 Scaling of droplet-substrate collisions

To represent the fully molten case, we apply scaling of the contact time to the viscous timescale of droplet-substrate collisions. We calculate the Ohnesorge number (Oh) to verify that the molten ash interactions will be dominated by viscous timescales ($Oh >> 1$) as opposed to inertial timescales ($Oh < 1$) (Kamp et al., 2017). The Ohnesorge number is described by:

$$Oh = \frac{\mu}{\sqrt{g\gamma R}}, \tag{4}$$

where g is the gravitational acceleration, R is the radius of the drop, γ is the surface tension, and μ is the viscosity of the melt (Kavehpour, 2015; Kamp et al., 2017). When applied to the Grey's Landing pyroclastic density current, the Ohnesorge number scales far greater than unity and viscous timescales dominate over inertial timescales (Kamp et al., 2017). Viscous timescales are calculated as (Kavehpour, 2015):

$$t_v = \frac{\mu R}{\gamma}, \tag{5}$$

and are on the order of 10^4 seconds for Grey's Landing.

We compare the time of contact to the viscous timescale with the assumption that if the contact time is larger than the viscous timescale, then the droplets will agglutinate (Figure 7).

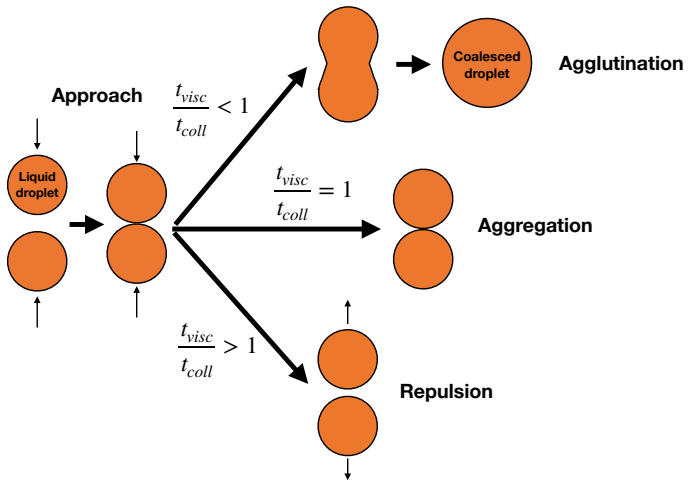

Figure 7: Illustration of the assumed collisional geometry in the timescale ratio scaling. Liquid droplets are assumed to collide head-on, and then either agglutinate if the viscous timescale is smaller than the collisional timescale, aggregate if the time scales are equal, or repel if the viscous.

We calculate the contact time of particles by:

$$t_{contact} = \pi \left(\frac{k}{m} - \frac{\eta^2}{4m^2} \right)^{-1/2}, \tag{6}$$

where k is the elastic coefficient , η is the normal dashpot damping coefficient, and m is the mass of the droplet (Silbert et al., 2001). We incorporate the influence of velocity and the particle diameter by:

$$t_{coll} = t_{contact} + \frac{2R}{u}, \tag{7}$$

As with the Gollwitzer et al. (2012) approach, we calculate a wide range of particle Reynolds and Stokes numbers for this timescale approach. The results, however, are in opposition with the Gollwitzer et al. (2012) scaling as the ratio of the viscous timescale to the collisional timescale is on the order of 10^5 to 10^6, meaning that the particles will rebound before they are able to deform and agglutinate (Figure 8).

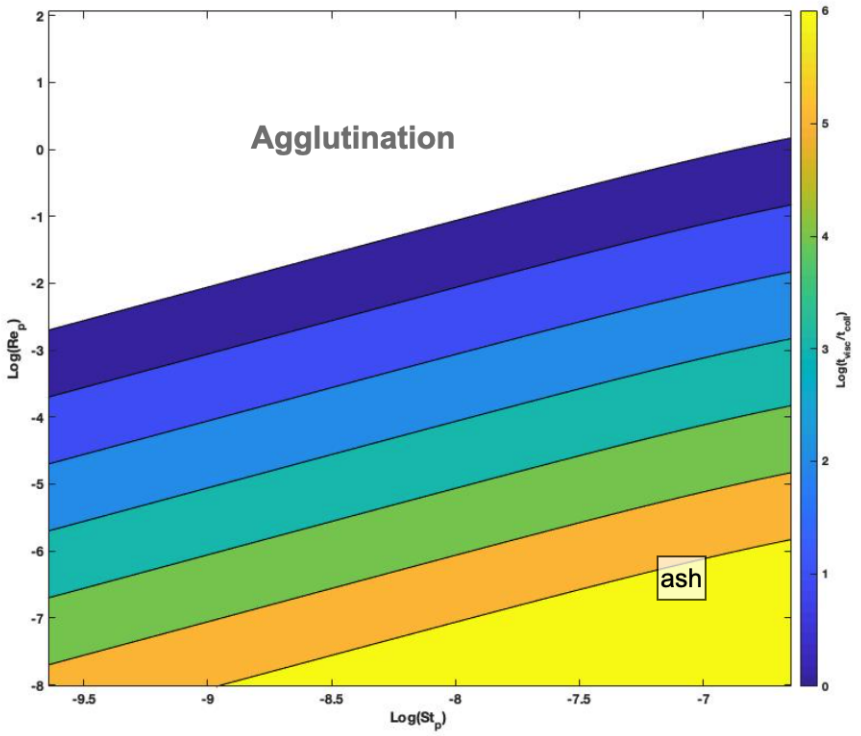

Figure 8: The ratio of the viscous timescale relative to the collisional timescale as a function of the particle Reynolds and Stokes numbers. Solid, molten, and partially-molten ash from Grey's Landing scales in the rebound space (represented by the color bar) where the timescale ratio is greater than 1.

Freundt (1998) conducted an experimental fluidization study in which they fluidized polyethyleneglycol (PEG) powder in perspex tanks with pumped air on the tank floor. The air was heated to raise powder beds to the melting temperature (47-64 °C) of the PEG powder. For the higher temperature experiments, at the melting temperature of PEG powder, they found the final bed consisted of dense solidified PEG melt at base overlain by welded crust that became increasingly less welded to fully unwelded with height from the base. They found rapid aggregation upon exceeding a critical melting temperature occurred for PEG powder particles. In that same study, Freundt (1998) also conducted turbulent flow experiments for PEG-spray suspensions. They found sedimentation to be influenced by droplet coalescence which generated large aggregates. The size of the PEG aggregates decreased with distance. The distal aggregates were formed by cooler PEG particles and were highly fragile. Freundt (1998) argues that aggregation and agglutination at the base of a pyroclastic density current would separate the flow into particulate transporting overflow and a viscous depositional underflow which grows through progressive aggradation (Branney and Kokelaar, 1992). They concluding that welding of high-grade ignimbrites includes pre-depositional aggregation, syndepositional aggradation and viscous deformation, through post-depositional shear and compaction. Freundt (1998) concludes that extensive high-grade ignimbrites cannot be formed by high-concentration pyroclastic density currents, as the particles would be sticky (supporting our Gollwitzer et al. (2012)-based scaling) and would

"catastrophically agglomerate" even at small coalescence efficiencies. Therefore, they argue these pyroclastic density currents are dilute with hot sticky particles (Freundt, 1998).

It would be beneficial for more studies on the interactions of partially-to-fully molten particle collisions to be conducted. There are limited studies thus far and they have involved typically extremely fine PEG powder that is finer that ignimbritic ash (Freundt, 1998). Isolating particles to study interactions and potential development of liquid bridges at different percent melt and collisional velocities would be fruitful to validate methods of scaling and to later be incorporated more accurately into multiphase models of pyroclastic density currents.

CHAPTER IV: AXISYMMETRIC, CONSTANT-VOLUME MODEL OF GREY'S LANDING PYROCLASTIC DENSITY CURRENT

We first approach modeling the pyroclastic density current with a simple numerical model, based off of the constant volume turbidity current model by Dade and Huppert (1995). We do this to get a sense of the parameter space before utilizing more complex models (see Chapter 5).The model considers an instantaneously well-mixed, fine-grained, axisymmetric gravity current released from a lock, which spreads radially over a non-erodible planar surface. To preserve a constant volume, entrainment is neglected in the model. The results of this box model inform a one-dimensional thermal model of an ignimbrite during deposition and throughout its post-depositional cooling by providing values for the initial volume of the PDC (V_o), duration of the flow, the runout of the flow ($x_{critical}$), the velocity of the current front (u), and the deposition rate (db/dt) of particles sedimenting out of the current (Dade and Huppert, 1995; Dade, 2003).

The volume of the pyroclastic density current remains constant; thus at any given time, the geometry relationship of the radially-spreading flow requires that:

$$V_o = \pi x^2 h, \tag{8}$$

where V_o is the initial and constant volume, x is the radial distance from the origin to the flow front, and h is the radially averaged thickness of the spreading

PDC. The volumetric particle concentration (ϕ) decreases with time as particles sediment out of the flow (Dade and Huppert, 1995). The runout of the PDC is marked by its buoyancy reversal. The runout distance ($x_{critical}$) is described by:

$$x_{critical} = ((1-\phi_{critical})^{1/2} - (\phi_{critical})^{1/2} arctan([(1-\phi_{critical})/\phi_{critical}]^{1/2}))^{0.3}, \quad (9)$$

where the critical concentration ($\phi_{critical}$) is (Dade and Huppert, 1995):

$$\phi_{critical} = \frac{\rho_a - \rho_i}{\rho_p - \rho_i}, \quad (10)$$

The flow rate of the radially spreading pyroclastic density current, u, is calculated by:

$$\frac{dx}{dt} = u = Fr[g'_p(\phi - \phi_{critical})]^{1/2}, \quad (11)$$

where

$$g'_p = \frac{g(\rho_p - \rho_i)}{\rho_a}, \quad (12)$$

and Fr is the Froude number, which is assumed to be a constant equal to the square root of 2 (Benjamin, 1968). The density of the ambient air, interstitial gas, and particles are given by ρ_a , ρ_i , and ρ_p , respectively. Throughout the flow of the PDC, particles sediment out, gradually creating the ignimbrite (Branney,

2002). Particles settle out of the current at a speed calculated by the Stokes settling velocity (w_s):

$$w_s = (2/9)\left(\frac{\rho_p - \rho_i}{\mu}\right) g(r^{1/2}), \tag{13}$$

where r is the radius of the particles (Robinson, 1926). The deposition rate of particles is:

$$\frac{db}{dt} = -\frac{w_s b}{h(4/3)\pi(d_p/2)^3}, \tag{14}$$

where b is the number of particles in the flow and d_p is the diameter of the particles in the pyroclastic density current. The initial number of particles in the flow, b_o, is calculated using the volume of the deposit and the diameter of the particles (Dade and Huppert, 1995):

$$b_o = \frac{V_s}{(4/3)\pi((d_p/2)^3)}, \tag{15}$$

where V_s is the volume of the solids, which for the Grey's Landing ignimbrite is calculated by:

$$V_s = V_{dep} - (V_{dep} * 0.075), \tag{16}$$

where V_{dep} is the volume of the Grey's Landing ignimbrite deposit. The 0.075 accounts for the porosity in the Grey's Landing ignimbrite (Lavallée et al., 2015).

As the constant volume pyroclastic density current travels radially outward from the caldera, the numerical model tracks the evolution of current height (h), volumetric particle concentration (ϕ), velocity of the current (u), number of particles in the flow (b), and the deposition rate (db/dt).

We utilize this model to illustrate the effects that initial particle volume concentration (volume fraction) and initial ash cloud volume (km^3) have on the runout distance of a pyroclastic density current (km) and its deposit volume (km). These results are not specific to an ignimbrite deposit and are meant to highlight the effect that particularly the initial particle concentration has on the pyroclastic density current and deposit. Figure 9 shows that increasing the initial volume fraction of particles and the volume of the initial ash cloud leads into increases in both the PDC runout and the deposit volume. However the runout distance is controlled more strongly by the initial ash cloud volume than by the initial volume fraction of particles

The general effect of pyroclastic density current volumetric particle concentration on the runout and deposit volume of an ignimbrite is shown in Figure 10.

We apply the Dade and Huppert (1995) axisymmetric, constant-volume gravity current model to the pyroclastic density current which produced the Grey's Landing ignimbrite (Andrews, 2011; Knott et al., 2020). We utilize minimum deposit area ($23,000\ km^2$) and volume ($2,800\ km^3$) of the Grey's Landing ignimbrite

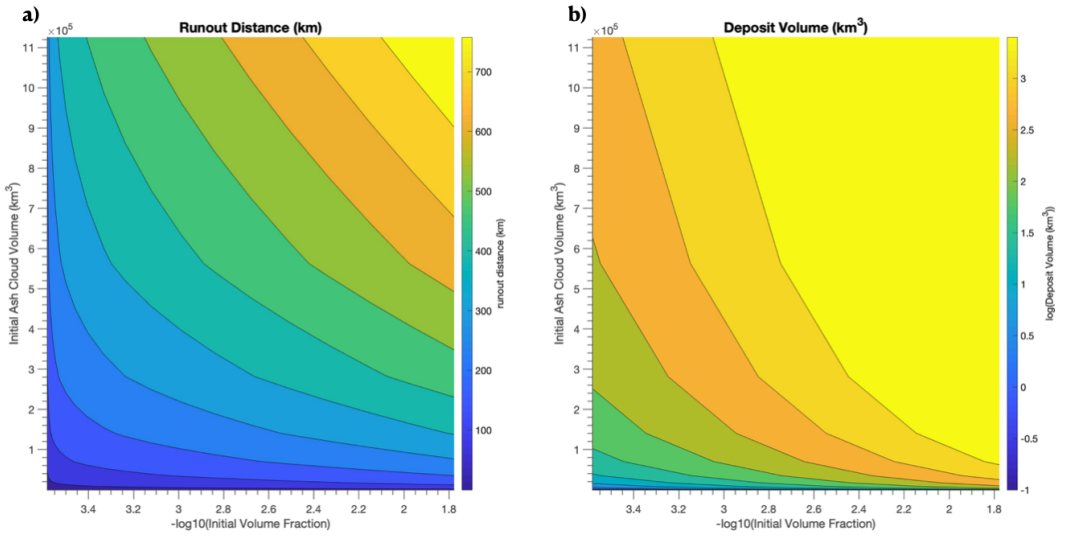

Figure 9: The effects of initial volume fraction and initial ash cloud volume on the runout distance of a pyroclastic density current and on the deposit volume.

estimated by Knott et al. (2020) to inform our calculations. There is no identifiable caldera at Grey's Landing (Andrews, 2011; Knott et al., 2020) therefore we follow the assumption made by Knott et al. (2020) of modest caldera dimensions of one tenth of the areal extent of Yellowstone, leading us to the assumption of initial PDC radius (x_1) of 5,000 meters.

Initial particle density (ρ_p) is calculated using the composition of the Grey's Landing ignimbrite (Andrews, 2011) in the program Rhyolite MELTS (Gualda et al., 2012; Ghiorso and Gualda, 2015), for temperatures ranging from 1400 °C to 650 °C. The Grey's Landing ignimbrite is broadly homogeneous in both bulk and glass compositions (Ellis et al., 2013, 2015). We tested a range of particle

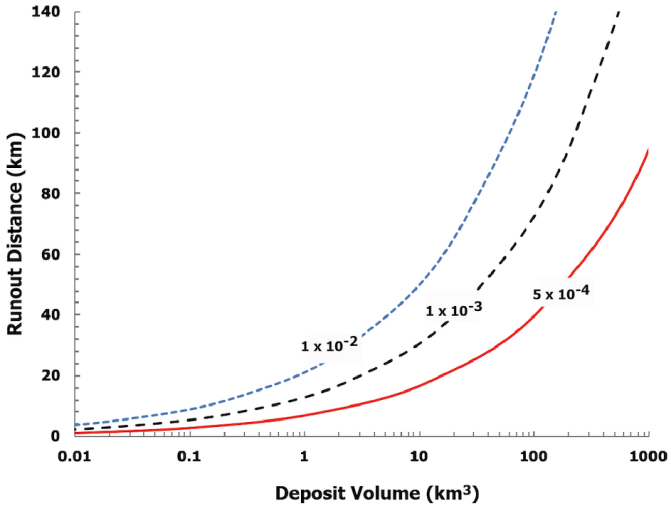

Figure 10: The effect of pyroclastic density current volumetric particle concentration on the runout and deposit volume of an ignimbrite from the constant-volume axisymmetric model.

diameters, from 1 x 10^{-4} to 1 x 10^{-2} meters. In the sieving of the rare, non-welded parts of large high-grade ignimbites in the Snake River Plain, including Grey's Landing, Branney et al. (2008) showed them to be fine-grained, free of pumice lapilli and fiamme, and better sorted than is typical for massive ignimbites. The high temperatures reached within the ignimbrite lead to melting of ash particles and resulted in the lava-like highly rheomorphic texture seen today (Andrews et al., 2008; Andrews, 2011; Lavallée et al., 2015; Robert et al., 2013).

Initial volumetric concentration and PDC temperature are the other unknown parameters within the model. We tested the initial volumetric concentration at three different values (0.01, 0.001, 0.0005) (Branney, 2002; Choux and Druitt,

2002) and tested temperatures over a range spanning 700 °C to 1,100 °C (Andrews, 2011; Manley and Andrews, 2004; Robert et al., 2013; Lavallée et al., 2015). The effects of temperature were found to be of negligible significance on flow dynamics relative to the inital volumetric concentration and particle diameter (Figure 11). A PDC temperature of 900 °C was therefore used for the model as it is close to the estimated emplacement temperature of the Grey's Landing vitrophyre (966 °C) (Lavallée et al., 2015).

The effects of particle diameter and initial volumetric concentration on the Grey's Landing pyroclastic density current are shown below in Figure 12, where the longest runout of the pyroclastic density current ($1.34x10^7$ meters) occurs with the smallest ash particle diameter ($1x10^{-4}$ meters), and the intermediate initial volumetric concentration (0.001). For all initial volumetric concentrations, the flows with the smallest particle diameters ($1x10^{-4}$ meters) had the longest runouts as well as had the largest amount of particles in the flow. We note that these results are substantially too large. The maximum runout at Grey's Landing is about 80 km from the center (Knott et al., 2020). The velocities recorded are physically unachievable in a pyroclastic density current (Figure 12).

The utility of the results is in a relative comparison of the effects of particle diameter, emplacement temperature, and initial volumetric concentration on an idealized "box model" flow. The current modeled is lacking integral parts of pyroclastic density current dynamics such as entrainment, cooling, or interactions

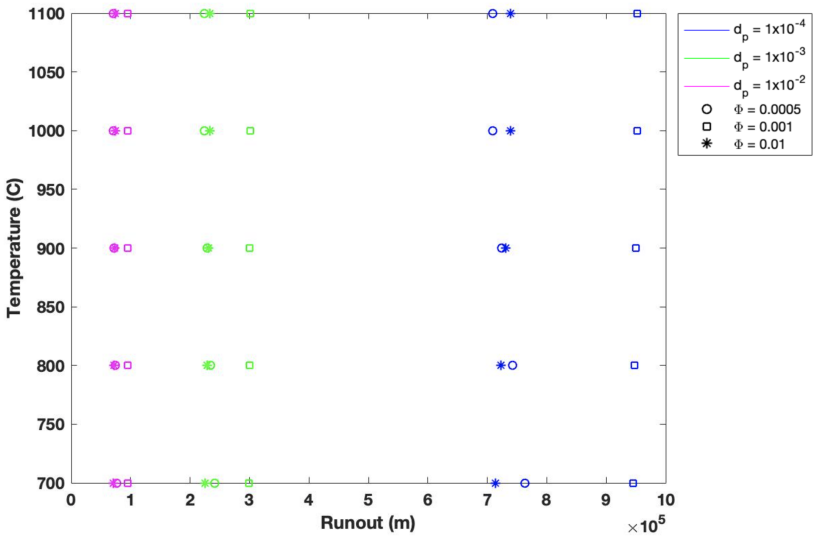

Figure 11: The relative effects of temperature, initial volumetric concentration, and ash particle diameter on the runout distance of the pyroclastic density current in the axisymmetric, constant volume numerical gravity current model. Blue markers represent runs with particle diameters of 1 x 10^{-4} meters, green represents runs with particle diameters of 1 x 10^{-3} meters, and magenta represents runs with particle diameters of 1 x 10^{-2} meters. Circular markers represent runs with initial volumetric concentration values of 0.005, squares are runs with initial volumetric concentration values of 0.001, and stars are runs with initial volumetric concentration values of 0.01.

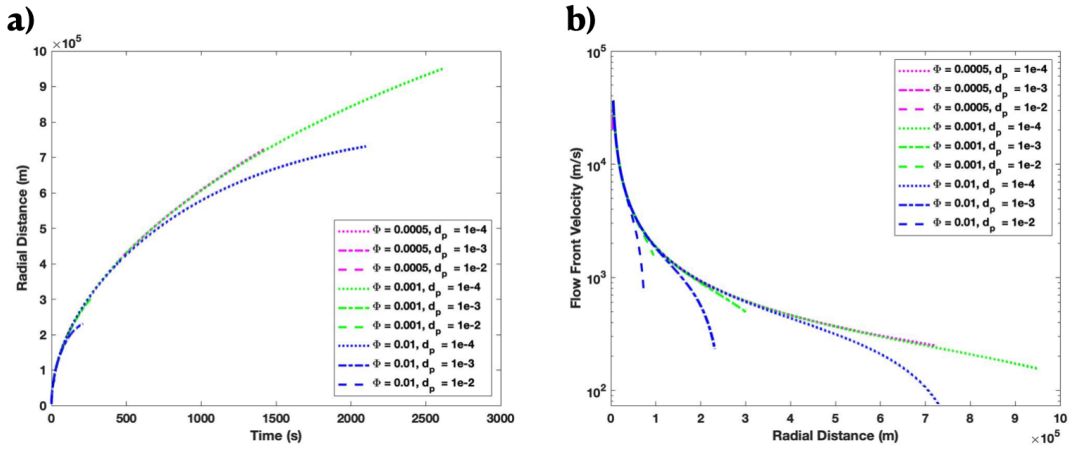

Figure 12: Resulting effects of ash particle diameter (1e-4, 1e-3, and 1e-3 meters) and initial volumetric concentration (0.0005, 0.001, and 0.01) on (a) the runout of the pyroclastic density current in the axisymmetric, constant volume numerical model and (b) the velocity of the flow. Temperature in all runs is 900 C

at the base of the flow (Roche et al., 2016; Andrews, 2014; Fauria et al., 2016; Sher and Woods, 2017).

CHAPTER V: MULTIPHASE MODEL OF A PYROCLASTIC DENSITY CURRENT THAT PRODUCES AN EXTREMELY HIGH-GRADE IGNIMBRITE

We model the pyroclastic density current which deposits the Grey's Landing ignimbrite with continuum multiphase models. Multiphase models are more realistic and capture flow dynamics more accurately than their box model counterparts, such as the axisymmetric, constant-volume model from Chapter 4 (Dufek and Bergantz, 2007). We utilize a Eulerian-Eulerian (EE) multiphase model in which the particle phase, treated as a fluid, and the carrier fluid phase, in this case it is air, have separate conservation equations for mass, momentum, and energy (Dufek and Bergantz, 2007).

The conservation of mass, or continuity, equation is written as:

$$\frac{\partial}{\partial t}({}^{m}\alpha\,{}^{m}\rho) + \frac{\partial}{\partial x_i}({}^{m}\alpha\,{}^{m}\rho\,{}^{m}U_i) = 0 \tag{17}$$

where ${}^{m}\alpha$ is the volume fraction of the mth phase (where if m=1 it is the gas phase and if m=2 it is the particle phase), ${}^{m}\rho$ is the density [kg/m^3] of the mth phase, ${}^{m}U_i$ is the average velocity [m/s] of the mth phase. The subscripts i and j are indices for spatial direction.

The conservation of momentum is calculated as:

$$\frac{\partial}{\partial t}({}^m\alpha^m\rho^m U_i) + \frac{\partial}{\partial x_j}({}^m\alpha^m\rho^m U_i^m U_j) = \frac{\partial^m P}{\partial x_i}\delta_{ij} + \frac{\partial^m \tau_{ij}}{\partial x_j} +^m I_i +^m \alpha^m \rho g_i \quad (18)$$

where ${}^mP$ is the pressure [Pa] of the mth phase, ${}^m\tau_{ij}$ is the stress tensor [Pa] of the mth phase, ${}^mI_i$ is the interphase momentum transfer [kg/m^3s], and g_i the gravitational acceleration [m/s^2].

The conservation of thermal energy is calculated as:

$${}^m\alpha^m\rho^m c_p\left(\frac{\partial^m T}{\partial t} +^m U_j\frac{\partial^m T}{\partial x_j}\right) = -\frac{\partial^m q}{\partial x_i} + H_{gp} \quad (19)$$

where ${}^mT$ is the thermal temperature [K]of the mth phase, ${}^mq$ is thermal heat flux [J/m^2s] of the mth phase, and H_{gp} is the interphase heat transfer [W/m^3].

In multiphase flows, separate boundary conditions must be specified for the continuous and particle phases. Here, we utilize the "leaky" boundary conditions (Dufek and Bergantz, 2007), in which all particles that reach the boundary are removed from the flow. This assumes the particles are perfectly sticky (no saltation at boundary) and become part of the substrate upon contact. This model reflect the Gollwitzer (2012) scaling of Grey's Landing ash particles shown in Chapter 3. We recognize this as an end-member case and further studies will need to be conducted either determine which scaling is more accurate or to model the effects of particles in which the viscous timescale is greater than the collisional timescale on the dynamics of the pyroclastic density current and subsequent deposit.

In order for the pyroclastic density current, with perfectly sticky ash particles, to reach the great extents seen in the Grey' Landing deposit, we assume the current is dilute ($\phi < 10^{-2}$) (Weit et al., 2018; Lube et al., 2020). In a dilute current, particle-particle interactions are rare and the transportation of particles in the current is dominated by fluid drag and gravity (Figure 13) (Lube et al., 2020). A dilute pyroclastic density current favors the propagation of the current if the particles are perfectly sticky as shown in the scaling from Chapter 3. Particles would be allowed to travel further because of the lack of coalescence and clustering that occurs during particle collisions. We note again that we utilize an end-member case here. Future studies may reveal that the scaling relationship between the viscous timescale and the collisional timescale is more accurate. In this case, the pyroclastic density current may not be dilute by necessity, as particles may "bounce" off one another and the substrate during collisions, allowing the current to potentially exist in an intermediate or dense regime (Breard et al., 2016; Lube et al., 2020).

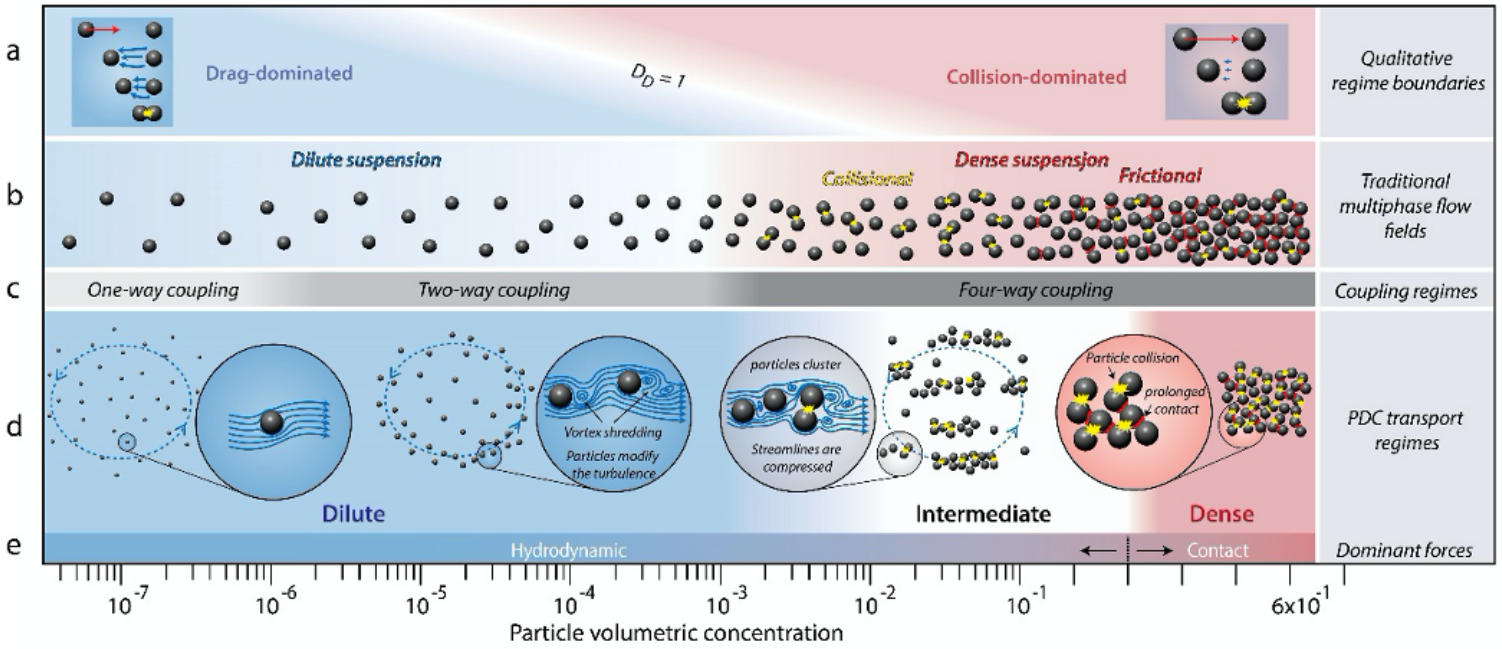

Figure 13: Delineating the dense, intermediate, and dilute transport regimes in pyroclastic density currents (figure originally from (Lube et al., 2020)).a) discriminating drag-dominated and collision-dominated transport regimes through a time-scale ratio not used in this study. b-c) a schematic presentation of the traditional multiphase flow fields of dilute and dense suspensions (b) and their associated gas-particle coupling regimes (c) relative to the flows' particle volume concentration. d) a schematic presentation and approximate range in particle concentration of the dilute, intermediate and dense transport regimes of PDCs. Details of gas-particle feedback mechanisms in each regime are highlighted in encircled 'zooms'. Blue arrows show fluid streamlines, blue dashed lines highlight large eddies. Yellow stars highlight particle collisions and their relative frequency. e) the threshold concentration at the intermediate-dense boundary where (frictional) contact stresses equals hydrodynamic stresses.

CHAPTER VI: THERMAL MODEL OF THE EVOLUTION OF AN EXTREMELY HIGH-GRADE IGNIMBRITE DURING AND AFTER DEPOSITION

We investigate the effects of strain heating on the temperatures in the Grey's Landing ignimbrite at various distances from the source. We also model the post-depositional cooling to determine if the deposit stays above the glass transition long enough for gravitational-induced flow, post-deposition, could significantly contribute to rheomorphism in the ignimbrite.

3 Construction of the thermal model

The general unsteady one-dimensional heat diffusion equation is described as:

$$\rho c \frac{\delta T}{\delta t} = \frac{\delta}{\delta y}\left(k \frac{\delta T}{\delta y}\right) + S, \tag{20}$$

where ρ is density, c is the heat capacity, and k is the conductivity of the material, T is temperature, t is time, y is the position, and S is a heat source term. Here, ρ and c are dependent on temperature. Thermal conductivity in rhyolites was shown by Romine et al. (2012) to vary little over a range of magmatic temperatures and water contents and is assumed here to be constant. The discretization of the one-dimensional unsteady heat diffusion equation in this study utilizes a fully implicit scheme. It is solved by the Tridiagonal Matrix Algorithm

(TDMA) for the temperature at each position in time, encompassing the unsteady heat diffusion as well as the thermal input from strain heating (Patankar, 1980). Following Patankar's (1980) derivations, the fully implicit discretization equation can be written as:

$$a_P T_P = a_S T_S + a_N T_N + b, \tag{21}$$

where

$$a_S = \frac{k_s}{(\partial y)_s}, \tag{22}$$

$$a_N = \frac{k_n}{(\partial y)_n}, \tag{23}$$

$$a_P^o = \frac{\rho c_p \Delta y}{\Delta t}, \tag{24}$$

$$b = S_c \Delta y + a_P^o T_P^o, \tag{25}$$

$$a_P = a_S + a_N + a_P^o - S_P \Delta y, \tag{26}$$

This series of equations represents the relationship, shown in Figure 14, between the temperature at point P (T_P) and its neighbors to the north (T_N) and

to the south (T_S) within the current time step, as well as their respective coefficients, and a linearized source term, b, which incorporates the coefficient a_P^o and the temperature of point P at the previous time step (T_P^o). The variables k_s and k_n refer to the conductivities at the interfaces. The locations of the parameters $(\partial y)_s$ and $(partialy)_n$ are shown in Figure 14. S_c, a constant external heat source, and S_P, an external heat force are set to zero in this study.

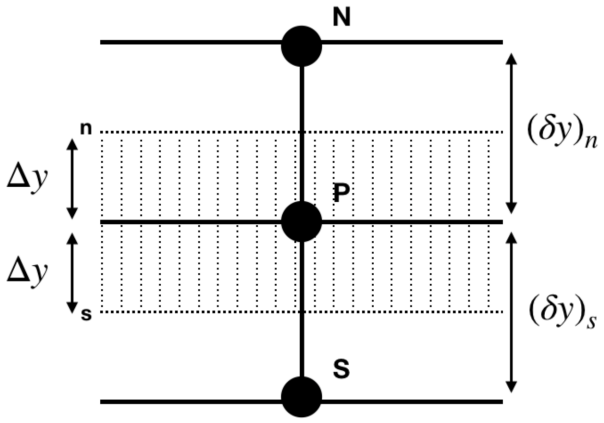

Figure 14: The one-dimensional heat diffusion discretization depicting node points P,S, and N; interfaces s and n, distances between nodes: $(\partial y)_n$ and $(\partial y)_s$, and the control volume Δy.

We calculate the influence of heating generated by viscous dissipation within the shear zone to investigate if the deposit undergoes significant strain to induce rheomorphism. Volumetric strain heating (Q_{strain}) in W/m^3, or the heat generated from viscous dissipation, is given by:

$$Q_{strain} = \eta \times \varepsilon^2, \tag{27}$$

where η is the apparent viscosity [Pa $\cdot$ s] and ε is the strain rate (Robert et al., 2013):

$$\varepsilon = \frac{\delta u}{\delta y}, \tag{28}$$

where u is the velocity in the pyroclastic density current and y the height of the current. We set the strain rate to exponentially decrease with depth from the top (the flow-substrate boundary) in the shear zone. The shear zone thickness (h_{sz}), which is vertically migrating during deposition) is set to be 2 meters in thickness (Andrews, 2006). The maximum shear zone thickness is 2 meters based on the wavelength ($\leq$ 1 m) of F_1 folds observed in the deposit and the maximum thickness ($\leq$ 1 m) of the folded layers in the ignimbrite (Andrews, 2011).

We calculate the increase in temperature (SP) at each node in the shear zone by:

$$SP = \frac{Q_{strain}\Delta t}{\rho c_p}, \tag{29}$$

using Q_{strain} $[W/m^3]$ at that node based on the temperatures and viscosities of the previous time step, the time step (Δt), and the density (ρ) $[kg/m^3]$ and heat capacity (c_p) [J/kgK] at that node which depend on the temperature of

the node at the previous time step. The values of density and heat capacity are determined from MELTS modeling of Grey's Landing and uses groupings of temperature as determined from the model to give temperature-dependent density and heat capacity. If the node is the newly emplaced node, representing the growing deposit through progressive aggradation, the viscosity, density, and heat capacity are based on the emplacement temperature.

We add this increase in temperature to the temperature of that node at the previous time step. The time steps are determined from an input file which gives information from the pyroclastic density current such as deposition rate [m/s],time [s], distance [m], shear rate [s^{-1}], and emplacement temperature [C].

The deposition of the Grey's Landing member is treated as a series of small, instantaneous emplacement events. The effects of compaction are neglected in the model for simplicity, but we note its importance on the welding of an ignimbrite (Quane and Russell, 2005).

The depositing ignimbrite, shown schematically in Figure 15, overlies a basal unit with a far-field temperature boundary held at 25 °C. The basal unit is defined by thermal properties different from those in the Grey's Landing ignimbrite. The density (ρ), heat capacity (c), thermal conductivity (k), and viscosity (μ) of the Grey's Landing deposit are assumed to be dependent on temperature. The liquidus was found to be at 1000.20 °C.

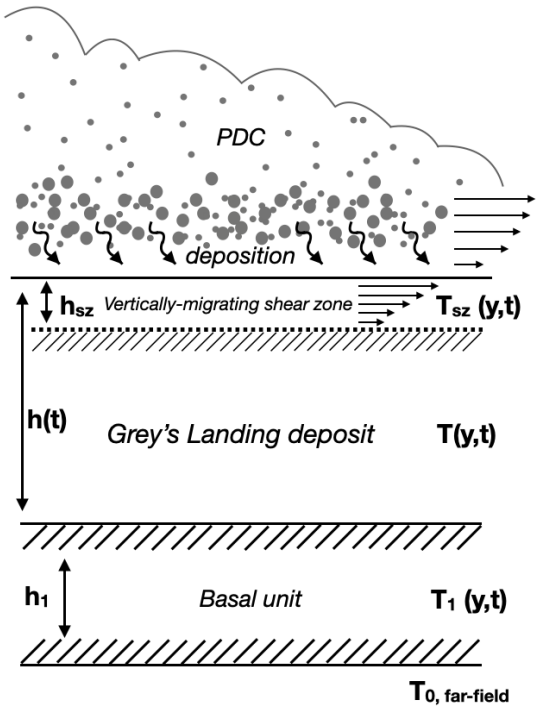

Figure 15: A visualization of the numerical model of the thermal evolution of the Grey's Landing ignimbrite through deposition. The basal unit is of a constant thickness (h_1) with a far-field temperature value (T_0) and its temperature varies in space and time (T_1). The Grey's Landing unit deposits in increments, as informed from the pyroclastic density current model. The thickness (h) of the deposit grows in time, and the temperature of the deposit (T) evolves in time and space. The vertically-migrating shear zone has a constant thickness (h_{sz}) and an evolving temperature (T_{sz}).

We utilize three different measurements of viscosity to calculate strain heating within the shear zone of Grey's Landing. In dilatometric measurement experiments performed in a study by Lavallée et al. (2015), the viscosity of Grey's Landing ignimbrite vitrophyre melt when temperatures are above the glass transition temperature (870 °C) and below 960 °C was found to be:

$$log_{10}(\eta) = \frac{9601}{T - 195.7} - 3.545, \tag{30}$$

Viscosity [Pa · s] is only included in the calculation of strain heating. We cap the upper limit of viscosity at the value for 960 ° C (Lavallée et al., 2015). When the temperature of a node is less than the glass transition temperature, we assume no strain heating occurs there.

We additionally calculate the thermal evolution of the Grey's Landing ignimbrite with the equation for viscosity as determined from parallel-plate viscometry experiments conducted by Robert et al. (2013) to measure the apparent viscosity of the basal Plinian ash-fall tuff at Grey's Landing. They found the apparent viscosity to be described by:

$$log_{10}(\eta) = \frac{13441}{T - 304.5} - 4.5, \tag{31}$$

We test another calculation of viscosity in the thermal model (Dufek and Bergantz, 2007), one in which the viscosity within the shear zone is assumed to

be the granular viscosity as outputted by the multiphase model:

$$ {}^{p}\mu = {}^{p}\ \mu^{f} + {}^{p}\ \mu^{k/c} \tag{32} $$

where ${}^{p}\mu^{f}$ is the effective viscosity in the frictional regime of the pyroclastic density current:

$$ {}^{p}\mu^{f} = \frac{P^{f} sin^{2p}\phi}{\sqrt{4sin^{2p}\phi^{p} I_{2D} + \left(\frac{\partial^{p} U_{i}}{\partial x_{i}}\right)^{2}}}, \tag{33} $$

where P^{f} is the frictional pressure, ${}^{p}\phi$ is the specularity, ${}^{p}I_{2D}$ is the second invariant of rate of strain tensor $[s^{-2}]$, ${}^{p}U_{i}$ is the average velocity of the particle phase [m/s] (Dufek and Bergantz, 2007). However, if the flow is dilute enough, this term contributes very little.

${}^{p}\mu^{k/c}$ is the total kinetic-collisional viscosity in the PDC and is described by:

$$ {}^{p}\mu^{k/c} = {}^{p}\ \alpha^{p}\rho\left({}^{p}v^{kin} + {}^{p}\ v^{coll}\right) \tag{34} $$

where ${}^{p}\alpha$ is the volume fraction of the particle phase, ${}^{p}\rho$ is the density of the particle phase $[kg/m^{3}]$, ${}^{p}v^{kin}$ is the kinetic shear viscosity, and ${}^{p}v^{coll}$ is the collisional shear viscosity (Dufek and Bergantz, 2007).

By testing the first two methods, we get a sense of the absolute maximum, but likely unrealistic strain heating possible with the viscosity from Equation 30 and Equation 31, and the minimum strain heating possible with the much lower

viscosity value of the granular viscosity.

Once the deposit has been fully emplaced, we calculate the diffusion timescale:

$$\tau = \frac{L^2}{K}, \tag{35}$$

where L is a characteristic length scale (here, the deposit thickness), and K is the thermal diffusivity which we calculate with the maximum density and heat capacity recorded in the deposit during emplacement. Once the deposit cools past the glass transition temperature (870 °C), it is assumed to be fully solidified and therefore rheomorphism will have ceased throughout the extent of the deposit (Lavallée et al., 2015). This assumed to occur within the diffusion timescale.

The models allow us to qualitatively investigate the thermal evolution of extremely high-grade ignimbrites, such as Grey's Landing, with the effects of strain heating during emplacement as well as calculate the post-depositional cooling. We will be able to determine if rheomorphism occurs predominately during emplacement of the ignimbrite, as a result of shearing, or it occurs primarily during post-depositional gravity-driven flow of the ignimbrite, as a result of the maintenance of high temperatures in the deposit.

4 General effects of velocity at the flow-substrate boundary and emplacement temperature on thermal evolution of a rheomorphic ignimbrite

We quantify the effects that emplacement temperature and velocity at the pyroclastic density current-substrate boundary have on the maximum amount of heat generated from strain at a single node and the time it takes for the ignimbrite to fully cool to the glass transition temperature (870 °C) (Lavallée et al., 2015).

First we test a range of volumetric particle concentrations for the pyroclastic density currents as well as particle size (given in diameter) on the deposition rate of the PDC (in m/s):

$$d = \frac{\phi w_s \Delta t}{\phi_d}, \tag{36}$$

where d is deposit thickness (in meters), ϕ is the volume fraction of particles in the flow, w_s is the settling velocity (m/s) which will be a function of particle diameter, Δt is the time interval (s), and ϕ_d is the volume fraction of particles in the deposit. We assume ϕ_d is one, meaning there is no pore space in the deposit. In actuality, the porosity of Grey's Landing is measured to be 0.77 (Lavallée et al., 2015). We plot the resultes of the calculations in Figure 16.

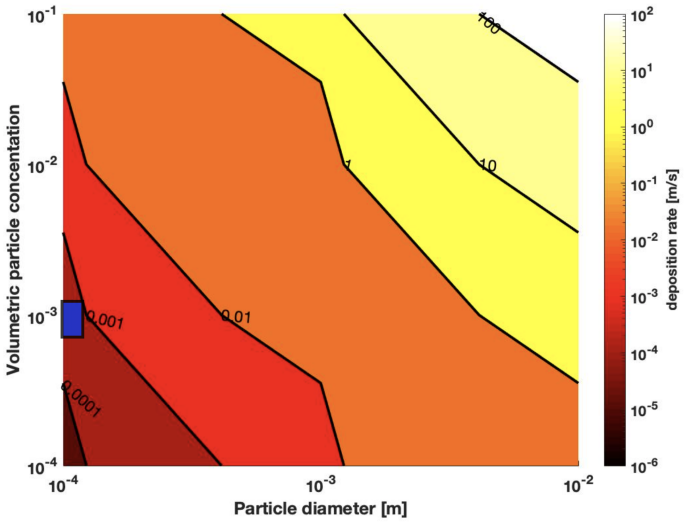

Figure 16: The ranges of possible deposition rates for the Grey's Landing pyroclastic density current as calculated from the volumetric particle concentration (ϕ) and the particle diameter (in meters). The blue region represents the selected deposition rate we used in created a regime diagram

The concentrations of the Grey's Landing PDC are unknown. We selected to use the deposition rate of 2.8x10^{-4} m/s produced by a volumetric particle concentration of 1 x 10^{-3} and a particle diameter of 100 microns. We selected a 100 micron particle diameter for our study as estimates of median diameter of grains at Grey's Landing is between 2-3 ϕ (125-250 micron) (Branney et al., 2008). More studies would need to be conducted in the future to determine which deposition rate is the most accurate. We chose a more dilute particle concentration since we are utilizing a perfectly sticky multiphase model in which particle agglutinate upon contact. A more dilute flow would allow particles to travel farther instead

of clustering and sedimenting out of the flow quickly and subsequently sticking to the boundary. Future studies should investigate the effects of different volumetric concentrations and particle-particle and particle-substrate collisions as describes in Chapter 3.

We compare unsteady one-dimensional thermal model results, with the deposition rate of 2.8x10^{-4} m/s, located one quarter (20 km) of the estimated furthest runout distance for the Grey's Landing PDC (Knott et al., 2020). We test the end-member maximum thermal effects of flow velocity at the current-substrate boundary and the emplacement temperature on the deposit. We utilize the viscosity (Equation 30 from Lavallée et al. (2015) in the calculation of strain heating. We approximate the strain rate here with the velocity at the flow-substrate boundary divided by the height of the deposit at that time. This does not include exponential decay as is described in Chapter 6 and executed in Chapter 7. This gives us the maximum possible strain heating and thus thermal effects. We test a velocity parameter space of 1, 0.1, 1 x 10^{-2}, 1 x 10^{-3}, 1 x 10^{-4}, and 1 x 10^{-5} m/s, and temperatures of 850, 900, 966 (the vitrophyre emplacement temperature found by Lavallée et al. (2015)), 1000, and 1050 °C to cover possible emplacement temperatures (Andrews, 2006, 2011; Robert et al., 2013; Ellis et al., 2015; Lavallée et al., 2015).

The effects of emplacement temperature and velocity at the flow-substrate boundary are shown in Figure 17. For all emplacement temperatures, a velocity

of 1 m/s produced substantial and physically unrealistic increases in temperature from strain heating; subsequently, the maximum increases in recorded temperature from the emplacement temperature and time for the entire deposit to cool to the glass transition temperature (870 °C) (Lavallée et al., 2015). These increases are the largest for the lowest emplacement temperature of 850 °C; where the maximum temperature increase from strain heating is $5.18\text{x}10^5$ °C, the maximum increase in temperature above the emplacement temperature is $4.88\text{x}10^5$ °C the cooling duration is 489 years. A velocity of 0.1 m/s creates an unrealistic value for an emplacement temperature of 850 °C such as generated increases in temperature from shearing at 1330 °C. However, for the other emplacement temperatures, the results are consistent with previous studies (Andrews, 2006, 2011; Robert et al., 2013; Ellis et al., 2015; Lavallée et al., 2015). We conclude that a velocity of 1 m/s is physically unrealistic and creates shear rates that are beyond what is likely possible for this type of flow. For this viscosity and shear rate this implies a 850 °C is also physically unrealistic. The value, being below that of the glass transition temperature, significantly effect viscosities in the deposit, leading to unrealistically high strain heating values, which the model assumes occurs regardless of the temperature. The ability to shear a deposit that it already below the suggested glass transition temperature Lavallée et al. (2015) would be difficult and unlikely. We conclude that the minimum possible emplacement temperature is the glass transition temperature.

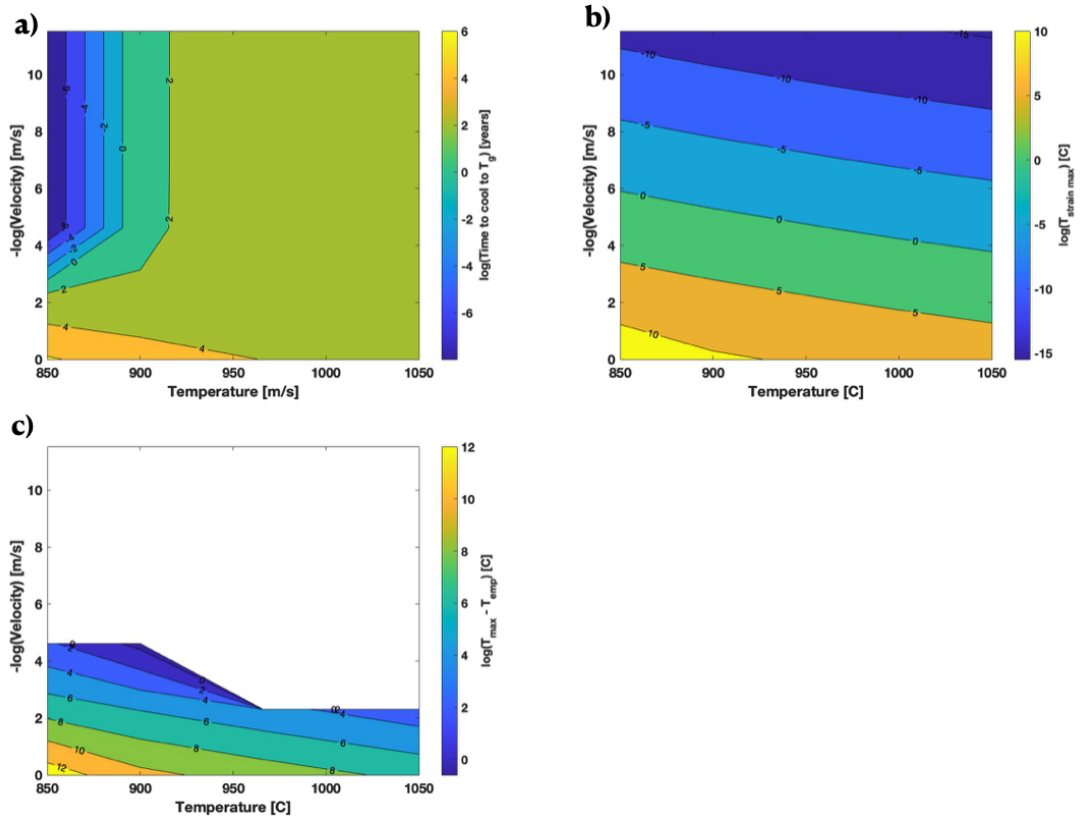

Figure 17: Effects of the velocity at the PDC-substrate boundary and the emplacement temperature on the heating and cooling of a Grey's Landing type deposit. Results were generated through a one-dimensional unsteady conduction model located 20 km from PDC source. The velocity at the boundary and the emplacement temperature did effect the thermal evolution on (a) the timescale (duration) for the deposit to fully cool to the glass transition temperature (870 °C; Lavallée et al. (2015)); (b) the maximum increase in temperature from strain heating; and (c) the maximum in increase of temperature (in Celsius) generated from strain heating.

When the emplacement temperature of 850 °C and the velocity of the flow at the flow-substrate boundary of 1 m/s are removed, the thermal effects of velocity and emplacement temperature are shown more clearly (Figure 18. The largest increases in temperature from strain heating and maximum increase of temperature relative to emplacement temperature occur at the larger velocities (e.g. 0.1 m/s) and lower temperatures (e.g. 900 °C). These results (Figure 17) suggest that there are effects from shearing in the deposit during deposition and those effects will change depending on the initial emplacement temperature and velocity at the flow-substrate boundary. However, we note again that these results are maximum possible strain heating. Previous studies have not investigated these effects before as they occur during progressive aggradation of the pyroclastic density current and particularly with thermal properties of the deposit that evolve with temperature (Andrews, 2006, 2011; Robert et al., 2013; Ellis et al., 2015; Lavallée et al., 2015).

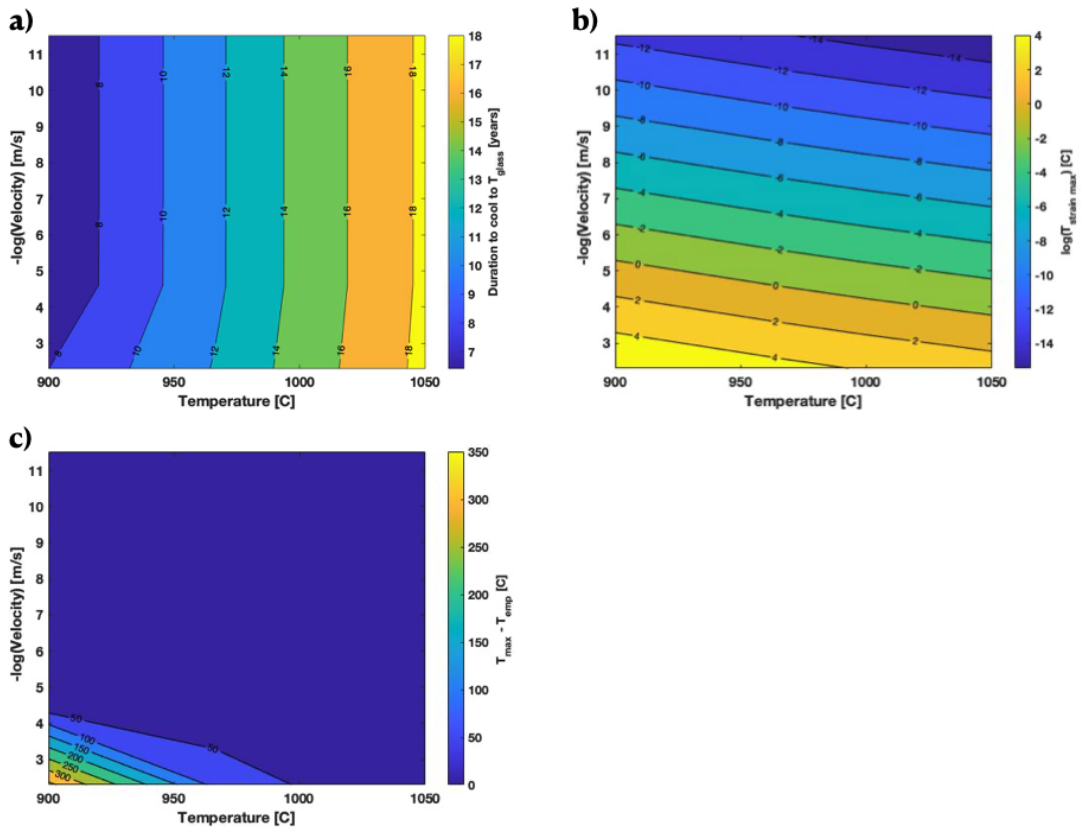

Figure 18: Effects of a narrower window of velocity at the PDC-substrate boundary and emplacement temperature on the heating and cooling of a Grey's Landing type deposit. Results were generated through a one-dimensional unsteady conduction model located 20 km from PDC source. The velocity at the boundary and the emplacement temperature did effect the thermal evolution on (a) the timescale (duration) for the deposit to fully cool to the glass transition temperature (870 °C; Lavallée et al. (2015)); (b) the maximum increase in temperature from strain heating; and (c) the maximum in increase of temperature (in Celsius) generated from strain heating.

CHAPTER VII: APPLICATION OF MODELS TO GREY'S LANDING PYROCLASTIC DENSITY CURRENT AND IGNIMBRITE

We apply our multiphase model and our thermal model to a Grey's Landing-type pyroclastic density current. The multiphase model, notably, does not include topography such as the western dipping floor of the Rogerson Graben or the Brown's Bench Escarpment. The modeled PDC flows over a flat, horizontal surface.

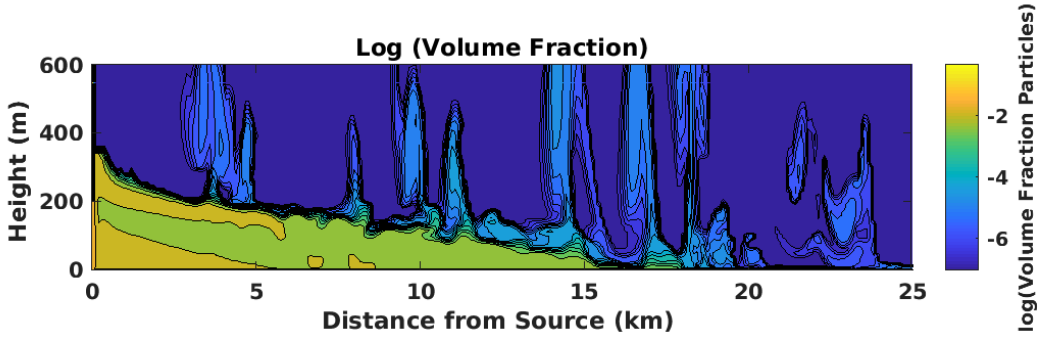

Figure 19: A snapshot of the Grey's Landing pyroclastic density current multiphase model during transport. The colorbar shows the log of the volume fraction of particles in the current at the time the snapshot was taken.

The multiphase model of the Grey's Landing pyroclastic density current (flow "snapshot" shown in Figure 19 utilizes a single grain size (125 micron), an initial volume fraction of 0.04, an initial height of 200 meters, an initial velocity of 20 m/s, and an initial temperature of 966 °C (the emplacement temperature of the Grey's Landing vitrophyre Lavallée et al. (2015)). The model ran for 3,158

seconds (approximately 52.6 minutes) and had a PDC runout distance of 59,900 meters. The runout distance is shorter than the longest runout (approximately 80 km) seen at Grey's Landing (Figure 1), but is consistent with the average runout (approximately 60 km).

We analyzed the results of the multiphase model at six distal locations (100, 1000, 10000, 20000, 30000, and 40000 meters from source) in order to assess the vertical thermal evolution of the deposit across extent of the ignimbrite. The subsequent deposit thinned and was emplaced at cooler temperatures with distance from the source, as is expected, shown in Figure 20.

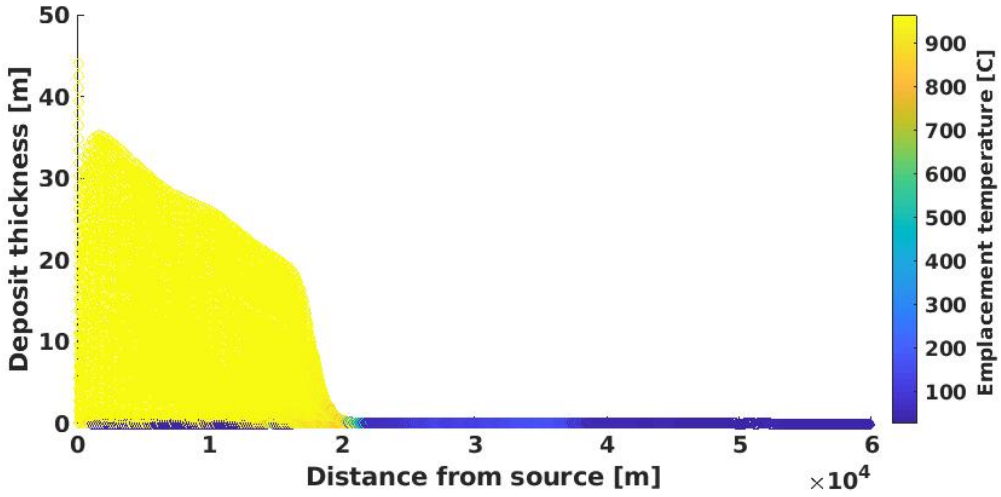

Figure 20: Grey's Landing ignimbrite deposit thickness as determined by the multiphase model. The colorbar shows emplacement temperature of the deposit .

We calculated the thermal evolution of the Grey's Landing PDC deposit, as informed by the multiphase model, three times - each with a different viscosity:

the viscosity of the vitrophyre measured by Lavallée et al. (2015), the viscosity of the basal ash fall measured by Robert et al. (2013), and the granular viscosity calculated in the multiphase model Dufek and Bergantz (2007), as described in Chapter 6. Figure 21 shows the vertical temperature profile following the cessation of emplacement, for each of the distal locations and for each of the viscosities (shown as subfigures).

The temperatures recorded in at the end of emplacement are effected by strain heating during emplacement, as the pyroclastic density current overrides the growing deposit, shearing the substrate. In Figure 22 we show (a) log of the maximum temperature increase in the ignimbrite at a node as a product of strain heating and viscosity calculation, (b) the ratio of the maximum increase in temperature at a node as a product of strain heating and the emplacement temperature, and (c) the log of the ratio of the maximum temperature recorded in the deposit at the end of emplacement and the emplacement temperature.

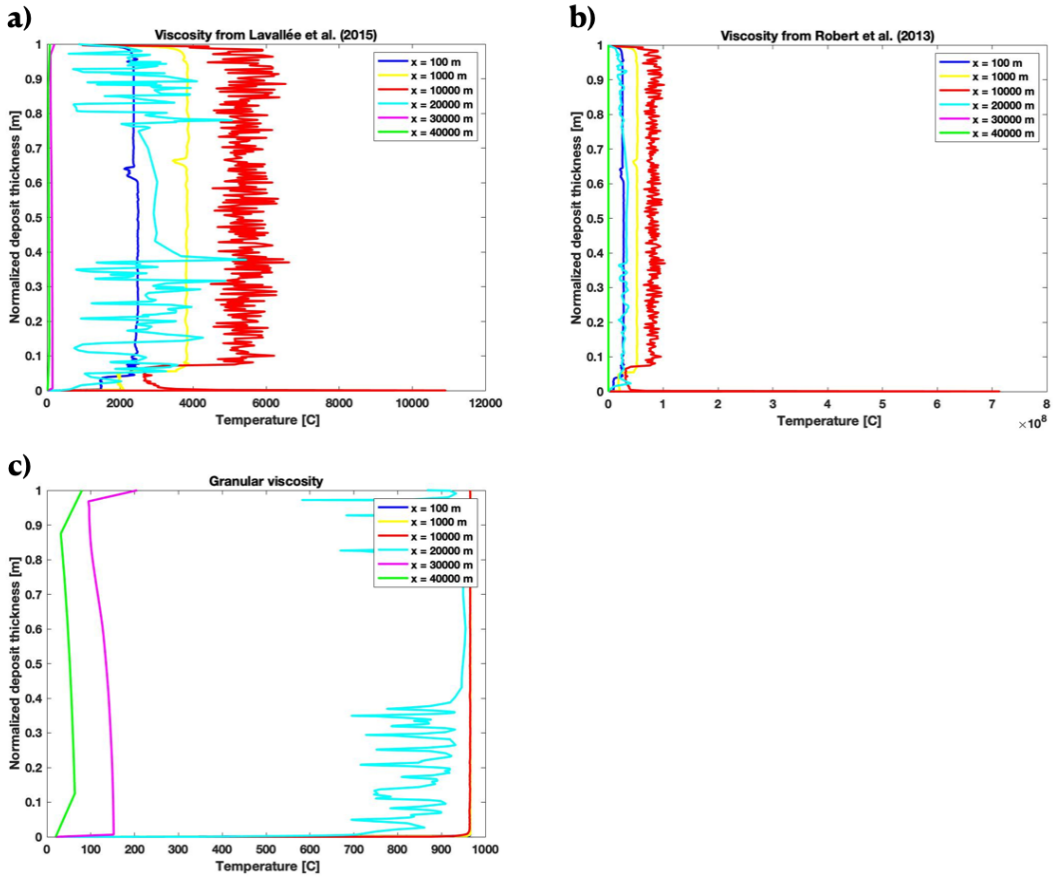

Figure 21: The vertical temperature profiles at the cessation of emplacement for six locations at different distances from the source, with normalized deposit thickness at each location. The temperature profiles from different calculations of viscosity in the shear zone are shown as separate subfigures: (a) viscosity of the Grey's Landing vitrophyre as calculated by Lavallée et al. (2015), (b) viscosity of the basal ash flow at Grey's Landing as calculated by Lavallée et al. (2015), and (c) granular viscosity calculated from the multiphase model of the Grey's Landing PDC.

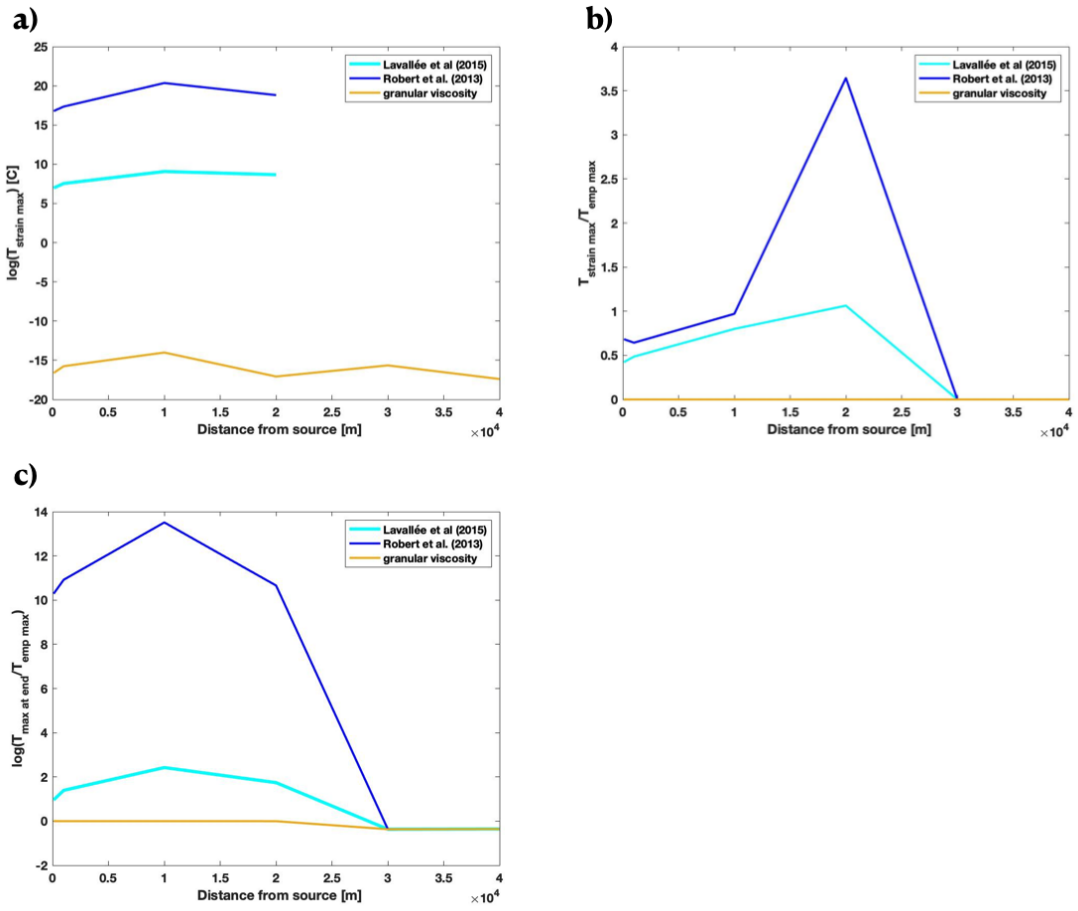

Figure 22: The increases in temperature in Grey's Landing ignimbrite as a product of strain heating. Each subfigure also shows the difference in these temperature increased based on the viscosity calculation within the two meter shear zone: where (a) log of the maximum temperature increase in the ignimbrite at a node as a product of strain heating and viscosity calculation, (b) the ratio of the maximum increase in temperature at a node as a product of strain heating and the emplacement temperature, and (c) the log of the ratio of the maximum temperature recorded in the deposit at the end of emplacement and the emplacement temperature.

The temperatures recorded in Grey's Landing were approximately 900-1100 °C. The maximum increases in temperature due to strain heating, as well as the maximum temperature recorded in the deposit is shown in Table 1 for 10 km from the PDC source.

	Lavallée et al. (2015)	Robert et al. (2013)	granular viscosity
T strain max (C)	8.73e3	6.93e8	0.82e-6
T max at end of emplacement (C)	1.09e4	7.14e8	965.73

Table 1: The values, recorded at 10 km from PDC source, of the maximum increases in temperature due to strain heating and the maximum temperature recorded in the deposit for Grey's Landing. Each column describes the results for a different method of calculating viscosity in the shear zone: viscosity measured by Lavallée et al. (2015), viscosity, measured by Robert et al. (2013), and the granular viscosity calculated from the multiphase model.

The increases in temperature as a product of strain heating are physically unrealistic for viscosity calculations in the shear zone for those measured by Lavallée et al. (2015) and Robert et al. (2013). The results from the Robert et al. (2013)

viscosity being orders of magnitude above temperatures recorded in Grey's Landing. The temperature increases from strain heating when granular viscosity is used are on the order of 10^{-8} to 10^{-10} and the changes to thermal evolution of the deposit relative to standard conduction from instantaneous emplacement are negligible.

We calculate the diffusion timescale for each x location from the source and present them in Figure 23. Diffusion timescale decreases with deposit thickness. We assume in this timescale, the temperatures will cool past the glass transition temperature. The diffusion timescale for the thicker regions is on the order of decades to nearly 140 years for the most proximal case. There is potential for the deposit to maintain heat long enough in the interior for rheomorphism to occur due to gravitation-induced flow.

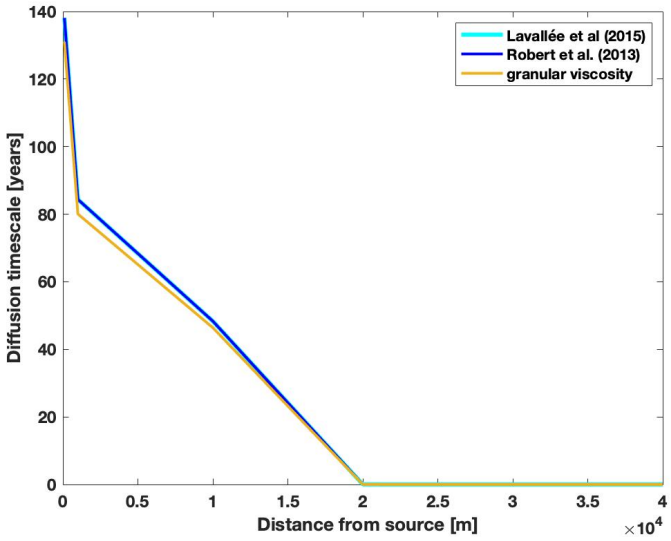

Figure 23: The diffusion timescale for Grey's Landing at varying distances from the source.

CHAPTER VIII: DISCUSSION

In the case of hot (966 °C), sticky ash particles which agglutinate upon contact in a dilute Grey's Landing pyroclastic density current, we find that the current is able to travel distances that match well with the average distal extents of the deposit (60 km from center). The eruption occurs in just under an hour and emplaces an ignimbrite as thick as 44.6 meters. We note the thickest area occurs very proximal to the source yet the maximum thickness produced by our model is less than half of the maximum thickness recorded in the actual Grey's Landing ignimbrite (approximately 100 m). However, Grey's Landing sits on top of a western sloping graben which may have contributed to deposit thickening particularly if high temperatures (above the glass transition) were maintained within the deposit.

The results of our thermal model support that vast majority of the interior of the ignimbrite could be held above the glass transition temperature for considerable periods of times; years in the thicker portion of the deposit where the emplacement temperature was above the glass transition temperature. The model, based on strain heating calculations using the granular viscosity determined by the multiphase model, generated virtually no temperature increases from strain heating for a starting temperature of the PDC of 966 °C. This, as well as the long cooling times, supports the hypothesis that the vast majority of rheomorphism

occurs post-deposition at Grey's Landing ignimbrite. More tests of this model at lower eruption and emplacement temperatures needs to occur to say more conclusively if strain heating could play a more substantial role. The general effects of strain heating model, shown in Chapter 6.2, imply that at cooler temperatures that are closer to the glass transition temperature, the temperature increases from strain heating become more significant.

CHAPTER IX: CONCLUSION

Our study is limited and does not cover the whole spectrum of studies that need to occur in order to fully characterize how ash agglutination effects the transport of the Grey's Landing pyroclastic density current, how the deposit reached it recorded temperatures of approximately 900-1000 °C, constrain all situations that could lead to shear heating, or include the topography of the underlying Rogerson Graben on the PDC flow and on post-depositional flow (Lavallée et al., 2015; Ellis et al., 2015; Andrews, 2011, 2006; Robert et al., 2013). Future studies would need to include: (1) experiments of partially-to-fully molten highly viscous particle-particle and particle-substrate collisions to better constrain under what conditions partially-to-fully molten ash agglutinates, (2) use the saltation boundary in the multiphase model to test the other end-member flow-substrate boundary effects, (3) use the experimental results and multiphase model to determine if the Grey's Landing pyroclastic density current needed to be dense or dilute, and (4) test a larger swathe of eruption and subsequently emplacement temperatures in the multiphase to fully constrain the effects of strain heating at Grey's Landing, (5) model the post-depositional cooling with fine resolution to determine how the deposit cools past the glass transition temperature.

REFERENCES

R. R. Almeev, T. Bolte, B. P. Nash, F. Holtz, M. Erdmann, and H. E. Cathey. High-temperature, low-H2O Silicic Magmas of the Yellowstone Hotspot: an Experimental Study of Rhyolite from the Bruneau–Jarbidge Eruptive Center, Central Snake River Plain, USA. *Journal of Petrology*, 53(9):1837–1866, sep 2012. ISSN 0022-3530. doi: 10.1093/petrology/egs035.

B. J. Andrews. Dispersal and air entrainment in unconfined dilute pyroclastic density currents. *Bulletin of Volcanology*, 76(9):852, 2014. ISSN 1432-0819. doi: 10.1007/s00445-014-0852-4.

B. M. J. Andrews, Graham D M. Emplacement and rheomorphic deformation of a large, lava-like rhyolitic ignimbrite: Grey's Landing, southern Idaho. *GSA Bulletin*, 123(3-4):725–743, 2011. ISSN 0016-7606. doi: 10.1130/B30167.1.

D. M. Andrews, Graham. *The emplacement and deformation of high-temperature tuffs: a structural analysis of the Grey's Landing ignimbrite, Snake River Plain, Idaho.* PhD thesis, University of Leicester, 2006.

G. D. M. Andrews, M. J. Branney, B. Bonnichsen, and M. McCurry. Rhyolitic ignimbrites in the Rogerson Graben, southern Snake River Plain volcanic province: volcanic stratigraphy, eruption history and basin evolution. *Bulletin of Volcanology*, 70(3):269–291, 2008. ISSN 1432-0819. doi: 10.1007/s00445-007-0139-0.

B. B and C. GP. The Cougar Point Tuff, southwestern Idaho. *Idaho Bur Min Geol Bull*, 26:255–281, 1982.

D. M. Bachmann, Olivier and P. Lipman. Voluminous lava-like precursor to a major ash-flow tuff: Low-column pyroclastic eruption of the Pagosa Peak Dacite, San Juan volcanic field, Colorado. *Journal of Volcanology and Geothermal Research - J VOLCANOL GEOTHERM RES*, 98, 2000. doi: 10.1016/S0377-0273(99)00185-7.

M. C. Benage, J. Dufek, and P. A. Mothes. Quantifying entrainment in pyroclastic density currents from the Tungurahua eruption, Ecuador: Integrating field proxies with numerical simulations. *Geophysical Research Letters*, 43(13):6932–6941, jul 2016. ISSN 0094-8276. doi: https://doi.org/10.1002/2016GL069527.

T. B. Benjamin. Gravity currents and related phenomena. 1968.

B. Bonnichsen, W. P. Leeman, N. Honjo, W. C. McIntosh, and M. M. Godchaux. Miocene silicic volcanism in southwestern Idaho: geochronology, geochemistry, and evolution of the central Snake River Plain. *Bulletin of Volcanology*, 70(3): 315–342, 2008. ISSN 1432-0819. doi: 10.1007/s00445-007-0141-6.

B. T. L. Branney, M J and M. Godchaux. Sheathfolds in rheomorphic ignimbrites. *Bulletin of Volcanology*, 66(6):485–491, 2004. ISSN 1432-0819. doi: 10.1007/s00445-003-0332-8.

K. P. Branney, M.J. Pyroclastic Density Currents and the Sedimentation of Ignimbrites. *Geol. Soc. London Mem.*, 27:1–143, 2002.

M. J. Branney and P. Kokelaar. A reappraisal of ignimbrite emplacement: progressive aggradation and changes from particulate to non-particulate flow during emplacement of high-grade ignimbrite. *Bulletin of Volcanology*, 54(6):504–520, 1992. ISSN 1432-0819. doi: 10.1007/BF00301396.

M. J. Branney and P. Kokelaar. Volcanotectonic faulting, soft-state deformation, and rheomorphism of tuffs during development of a piecemeal caldera, English Lake District. *GSA Bulletin*, 106(4):507–530, apr 1994. ISSN 0016-7606. doi: 10.1130/0016-7606(1994)106¡0507:VFSSDA¿2.3.CO;2.

M. J. Branney, B. Bonnichsen, G. D. M. Andrews, B. Ellis, T. L. Barry, and M. McCurry. 'Snake River (SR)-type' volcanism at the Yellowstone hotspot track: distinctive products from unusual, high-temperature silicic super-eruptions. *Bulletin of Volcanology*, 70(3):293–314, 2008. ISSN 1432-0819. doi: 10.1007/s00445-007-0140-7.

E. C. P. Breard, G. Lube, J. R. Jones, J. Dufek, S. J. Cronin, G. A. Valentine, and A. Moebis. Coupling of turbulent and non-turbulent flow regimes within pyroclastic density currents. *Nature Geoscience*, 9(10):767–771, 2016. ISSN 1752-0908. doi: 10.1038/ngeo2794. URL `https://doi.org/10.1038/ngeo2794`.

H. E. Cathey and B. P. Nash. The Cougar Point Tuff: Implications for Thermochemical Zonation and Longevity of High-Temperature, Large-Volume Silicic Magmas of the Miocene Yellowstone Hotspot. *Journal of Petrology*, 45(1):27–58, jan 2004. ISSN 0022-3530. doi: 10.1093/petrology/egg081.

L. G. Chapin, C.E. Primary and secondary flow structures in ash-fl ow tuffs of the Gribbles Run paleovalley, central Colorado. *Ash-Flow Tuffs: Geological Society of America Special Paper*, 180:137–154, 1979. doi: 10.1130/SPE180-p137.

A. Chesters. The modelling of coalescence processes in fluid-liquid dispersions : a review of current understanding. *Chemical Engineering Research and Design*, 69(A4):259–270, 1991. ISSN 0263-8762.

C. M. Choux and T. H. Druitt. Analogue study of particle segregation in pyroclastic density currents, with implications for the emplacement mechanisms of large ignimbrites. *Sedimentology*, 49(5):907–928, oct 2002. ISSN 0037-0746. doi: https://doi.org/10.1046/j.1365-3091.2002.00481.x.

W. B. Dade. The emplacement of low-aspect ratio ignimbrites by turbulent parent flows. *Journal of Geophysical Research: Solid Earth*, 108(B4), 2003. doi: 10.1029/2001JB001010.

W. B. Dade and H. E. Huppert. Runout and fine-sediment deposits of axisym-

metric turbidity currents. *Journal of Geophysical Research: Oceans*, 100(C9): 18597–18609, 1995. doi: 10.1029/95JC01917.

J. Dufek and G. W. Bergantz. Suspended load and bed-load transport of particle-laden gravity currents: the role of particle–bed interaction. *Theoretical and computational fluid dynamics*, 21(2):119–145, 2007. ISSN 0935-4964. doi: 10.1007/s00162-007-0041-6.

E. Ekren, D. McIntyre, and E. Bennett. High- temperature, large-volume, lavalike ash-flow tuffs without calderas in southwestern Idaho. *U.S. Geological Survey Professional Paper*, 1272, 1984.

B. S. Ellis, J. A. Wolff, S. Boroughs, D. F. Mark, W. A. Starkel, and B. Bonnichsen. Rhyolitic volcanism of the central Snake River Plain: a review. *Bulletin of Volcanology*, 75(8):745, 2013. ISSN 1432-0819. doi: 10.1007/s00445-013-0745-y.

B. S. Ellis, B. Cordonnier, M. C. Rowe, D. Szymanowski, O. Bachmann, and G. D. M. Andrews. Groundmass crystallisation and cooling rates of lava-like ignimbrites: the Grey's Landing ignimbrite, southern Idaho, USA. *Bulletin of Volcanology*, 77(10):87, 2015. ISSN 1432-0819. doi: 10.1007/s00445-015-0972-5.

K. E. Fauria, M. Manga, and M. Chamberlain. Effect of particle entrainment on the runout of pyroclastic density currents. *Journal of Geophysical*

Research: Solid Earth, 121(9):6445–6461, sep 2016. ISSN 2169-9313. doi: https://doi.org/10.1002/2016JB013263.

A. Freundt. The formation of high-grade ignimbrites: Part I. Experiments on high- and low-concentration transport systems containing sticky particles. *Bulletin of Volcanology*, 59:414–435, 1998. doi: 10.1007/ s004450050201.

A. Freundt. Formation of high-grade ignimbrites Part II. A pyroclastic suspension current model with implications also for low-grade ignimbrites. *Bulletin of Volcanology*, 60(7):545–567, 1999. ISSN 1432-0819. doi: 10.1007/s004450050251.

M. S. Ghiorso and G. A. R. Gualda. An H2O–CO2 mixed fluid saturation model compatible with rhyolite-MELTS. *Contributions to Mineralogy and Petrology*, 169(6):53, 2015. ISSN 1432-0967. doi: 10.1007/s00410-015-1141-8.

F. Gollwitzer, I. Rehberg, C. A. Kruelle, and K. Huang. Coefficient of restitution for wet particles. *Physical Review E*, 86(1):11303, 2012. doi: 10.1103/PhysRevE.86.011303.

G. A. R. Gualda, M. S. Ghiorso, R. V. Lemons, and T. L. Carley. Rhyolite-melts: a modified calibration of melts optimized for silica-rich, fluid-bearing magmatic systems. *Journal of Petrology*, 53(5):875–890, 01 2012. ISSN 0022-3530. doi: 10.1093/petrology/egr080.

A. P. Janssen, P.J.A. *Macromolecular Materials and Engineering*, 296(3-4):238–248, 2011. ISSN 1438-7492. doi: 10.1002/mame.201000375.

J. Kamp, J. Villwock, and M. Kraume. Drop coalescence in technical liquid/liquid applications: A review on experimental techniques and modeling approaches. *Reviews in Chemical Engineering*, 33:1, 02 2017. doi: 10.1515/revce-2015-0071.

H. P. Kavehpour. Coalescence of Drops. *Annual Review of Fluid Mechanics*, 47 (1):245–268, 2015. ISSN 0066-4189. doi: 10.1146/annurev-fluid-010814-014720.

L. A. Kirstein, C. J. Hawkesworth, and F. G. Garland. Felsic lavas or rheomorphic ignimbrites: is there a chemical distinction? *Contributions to Mineralogy and Petrology*, 142(3):309–322, 2001. ISSN 1432-0967. doi: 10.1007/s004100100291.

T. R. Knott, M. K. Reichow, M. J. Branney, D. R. Finn, R. S. Coe, M. Storey, and B. Bonnichsen. Rheomorphic ignimbrites of the Rogerson Formation, central Snake River plain, USA: record of mid-Miocene rhyolitic explosive eruptions and associated crustal subsidence along the Yellowstone hotspot track. *Bulletin of Volcanology*, 78(4):23, 2016. ISSN 1432-0819. doi: 10.1007/s00445-016-1003-x.

T. R. Knott, M. J. Branney, M. K. Reichow, D. R. Finn, S. Tapster, and R. S. Coe. Discovery of two new super-eruptions from the Yellowstone hotspot track (USA): Is the Yellowstone hotspot waning? *Geology*, jun 2020. ISSN 0091-7613. doi: 10.1130/G47384.1.

Y. Lavallée, F. B. Wadsworth, J. Vasseur, J. K. Russell, G. D. M. Andrews, K.-U. Hess, F. W. von Aulock, J. E. Kendrick, H. Tuffen, A. J. Biggin, and D. B. Dingwell. Eruption and emplacement timescales of ignimbrite super-eruptions from thermo-kinetics of glass shards . *Frontiers in Earth Science*, 3, 2015.

G. Lube, E. C. P. Breard, T. Esposti-Ongaro, J. Dufek, and B. Brand. Multiphase flow behaviour and hazard prediction of pyroclastic density currents. *Nature Reviews Earth & Environment*, 1(7):348–365, 2020. ISSN 2662-138X. doi: 10.1038/s43017-020-0064-8.

C. Manley and G. Andrews. A numerical modelling investigation of the duration of post-emplacement rheomorphism in a high-grade ignimbrite: Grey's Landing, Idaho. *Geological Society of America Abstracts with Programs*, 36:12, 2004.

C. R. Manley. Extended cooling and viscous flow of large, hot rhyolite lavas: implications of numerical modeling results. *Journal of Volcanology and Geothermal Research*, 53(1):27–46, 1992. ISSN 0377-0273. doi: https://doi.org/10.1016/0377-0273(92)90072-L.

B. Nash, M. E. Perkins, J. N. Christensen, D. Lee, and A. Halliday. The yellowstone hotspot in space and time: Nd and hf isotopes in silicic magmas. *Earth and Planetary Science Letters*, 247:143–156, 2006.

S. L. Quane and J. Russell. Welding: insights from high-temperature analogue

experiments. *Journal of Volcanology and Geothermal Research*, 142(1-2):67–87, apr 2005. ISSN 0377-0273. doi: 10.1016/J.JVOLGEORES.2004.10.014.

G. Robert, G. D. M. Andrews, J. Ye, and A. G. Whittington. Rheological controls on the emplacement of extremely high-grade ignimbrites. *Geology*, 41(9):1031–1034, 2013. ISSN 0091-7613. doi: 10.1130/G34519.1.

C. D. Robinson. Some Factors Influencing Sedimentation. *Industrial & Engineering Chemistry*, 18(8):869–871, 1926. ISSN 0019-7866. doi: 10.1021/ie50200a036.

O. Roche, D. C. Buesch, and G. A. Valentine. Slow-moving and far-travelled dense pyroclastic flows during the Peach Spring super-eruption. *Nature Communications*, 7(1):10890, 2016. ISSN 2041-1723. doi: 10.1038/ncomms10890.

W. L. Romine, A. G. Whittington, P. I. Nabelek, and A. M. Hofmeister. Thermal diffusivity of rhyolitic glasses and melts: effects of temperature, crystals and dissolved water. *Bulletin of Volcanology*, 74(10):2273–2287, 2012. ISSN 1432-0819. doi: 10.1007/s00445-012-0661-6.

H. U. Schmincke. Volcanological aspects of peralkaline silicic welded ash-flow tuffs. *Bulletin Volcanologique*, 38(2):594–636, 1974. ISSN 1432-0819. doi: 10.1007/BF02596900.

D. Sher and A. W. Woods. Experiments on mixing in pyroclastic density currents generated from short-lived volcanic explosions. *Earth and*

Planetary Science Letters, 467:138–148, 2017. ISSN 0012-821X. doi: https://doi.org/10.1016/j.epsl.2017.03.009.

L. E. Silbert, D. Erta, G. S. Grest, T. C. Halsey, D. Levine, and S. J. Plimpton. Granular flow down an inclined plane: Bagnold scaling and rheology. *Phys. Rev. E*, 64:051302, 2001. doi: 10.1103/PhysRevE.64.051302.

M. J. Streck and A. L. Grunder. Crystallization and welding variations in a widespread ignimbrite sheet; the Rattlesnake Tuff, eastern Oregon, USA. *Bulletin of Volcanology*, 57(3):151–169, 1995. ISSN 1432-0819. doi: 10.1007/BF00265035.

J. Telling and J. Dufek. An experimental evaluation of ash aggregation in explosive volcanic eruptions. *Journal of Volcanology and Geothermal Research*, 209-210: 1–8, 2012. ISSN 0377-0273. doi: 10.1016/J.JVOLGEORES.2011.09.008.

A. Weit, O. Roche, T. Dubois, and M. Manga. Experimental Measurement of the Solid Particle Concentration in Geophysical Turbulent Gas-Particle Mixtures. *Journal of Geophysical Research: Solid Earth*, 123(5):3747–3761, 2018. doi: https://doi.org/10.1029/2018JB015530.

*APPENDIX A. Validation of axisymmetric, constant-volume PDC model

A validation of the axisymmetric, constant-volume gravity current numerical model based on that of Dade and Huppert (1995) was undertaken to ensure the model captured physically accurate behavior. The model, which considers an instantaneously well-mixed, fine grained, axisymmetric gravity current released from a lock which spreads radially over a non-erodible planar surface, is compared to experiments conducted by Bonnecaze et al. (1995) in which silicon carbide particles were released from a semi-circular lock with a 10 cm radius into a water-filled rectangular tank with dimensions of 150 cm by 250 cm and a water depth of 14 cm. The schematic is shown below in Figure 24

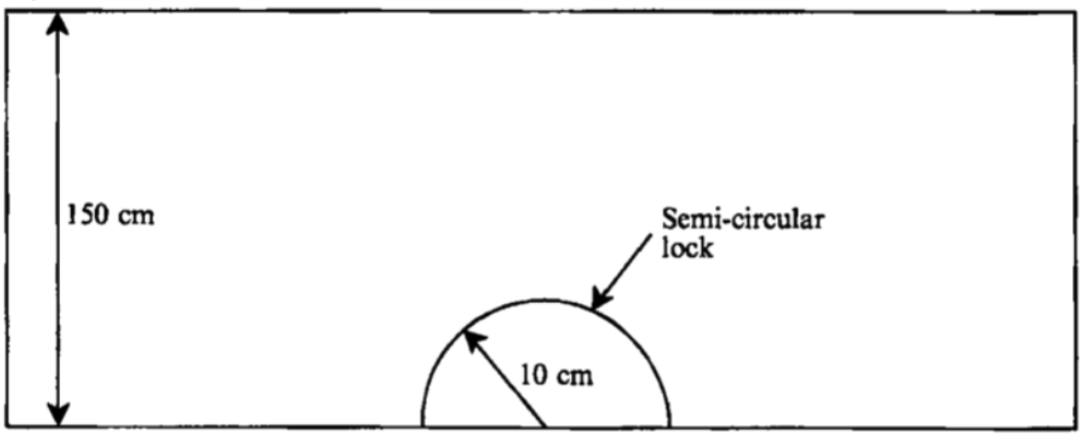

Figure 24: Schematic from Bonnecaze et al. (1995) depicting a large rectangular experimental water-filled tank with a semi-circular lock used in experiments on constant-volume currents.

Particle density (ρ) was 3217 kg/m^3 and particle diameter (d_p) was 37 mi-

crons. Initial volume (V_O) of the current was 0.006874 m^3 with an assumed initial temperature of 25 C. Initial volume fraction (ϕ) was 0.2. The model was set to have spatial steps of 0.01 meter. In the experiment and the model, the critical concentration (phi_{crit}) was assumed to be zero.

Comparisons between the theoretical predictions of the model and the experimental results from Bonnecaze et al. (1995) are presented in Table 2 where the runout distance (in meters) and the settling velocity of the particles matches well between the model and experiments.

	Numerical model	Bonnecaze et al. (1995) experiment
Runout distance (m)	0.77	0.76
Settling velocity (m/s)	1.7e-3	1.5e-3

Table 2: Comparison of Bonnecaze et al. (1995) constant volume gravity current experiements and axisymmetric, constant volume numerical model results based on Dade and Huppert (1995)

The non-dimensionalized numerical model results for the Bonnecaze et al.(1995) experiments are shown in Figure 25.

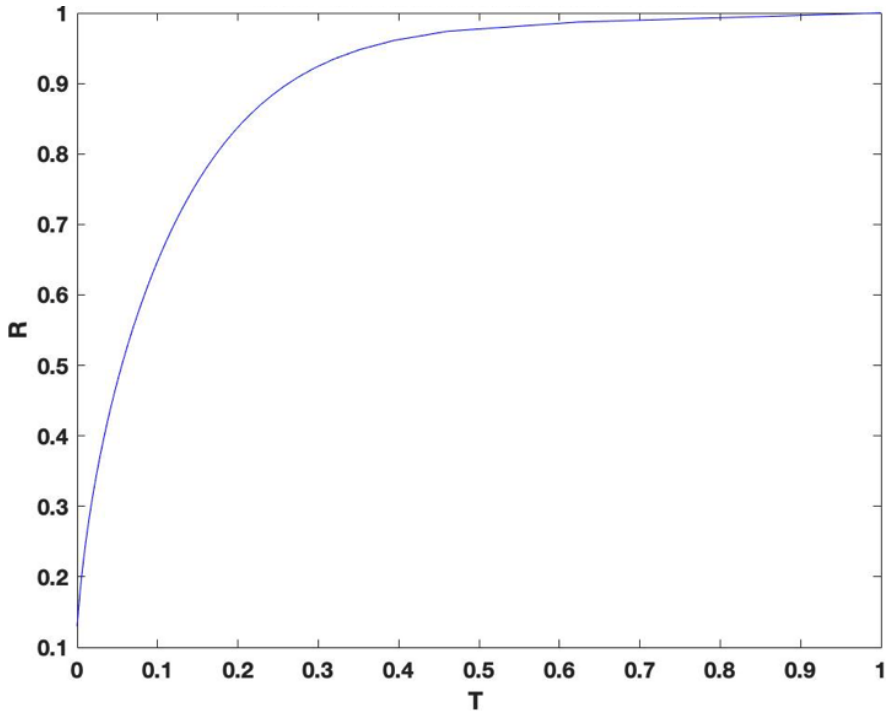

Figure 25: The runout of the axisymmetrically spreading gravity current follows the instantaneous release of dense suspensions with constant volume. The figure shows the dimensionless distance, $R = r/r_\infty$, as a function of the dimensionless time, $T = t/t_\infty$ of the numerical axisymmetric, constant-volume gravity current model using the geometries and experiemental values from Bonnecaze et al. (1995)